A Regeneratively Modelocked, Fiber Ring Laser

by

Matthew Edward Grein

Submitted to the Department of Electrical Engineering and Computer Science
in partial fulfillment of the requirements for the degree of

Master of Science in Electrical Engineering and Computer Science

at the

MASSACHUSETTS INSTITUTE OF TECHNOLOGY

September 1997

Author .....
Department of Electrical Engineering and Computer Science
August 25, 1997

Certified by .....
Erich P. Ippen
Elihu Thomson Professor of Electrical Engineering
Thesis Supervisor

Accepted by .....
Arthur C. Smith
Chairman, Department Committee on Graduate Students

A Regeneratively Modelocked, Fiber Ring Laser

by

Matthew Edward Grein

Submitted to the Department of Electrical Engineering and Computer Science
on August 25, 1997, in partial fulfillment of the
requirements for the degree of
Master of Science in Electrical Engineering and Computer Science

Abstract

This thesis addresses some of the issues relating to the construction of a regeneratively modelocked, fiber ring laser for high repetition rates. The equations governing feedback are derived, and experimental performance of the system with various filter bandwidths are given. The results are compared with those of active modelocking without stabilization. Pulse stabilization in the actively modelocked laser is reviewed, and a comparison between three mechanisms exhibiting pulsewidth-dependent loss (spectral limiting)–sideband limitng, SPM + filtering, and modulator-induced losses– is discussed. Motivation and a plan for future work are outlined.

Thesis Supervisor: Erich P. Ippen
Title: Elihu Thomson Professor of Electrical Engineering

Acknowledgments

Of the many to whom I owe this bit of written acknowledgment, my debts are greatest to my thesis and research advisor, Professor Ippen. It has been a great pleasure to work with him over the last two years–his is an insight colored by deep physical intuition, and his solid belief in his students and demand for excellence is inspiring. He has taught me much about life's many lessons, both inside and outside of the laboratory, and I look forward to his continued guidance and support. I have enjoyed working with Professor Haus and speaking with him on much of the material in this thesis. His sharp intellect tempered with humor is both compelling and encouraging.

Of the many students and colleagues that I'd like to acknowledge for their support, a few are most noteworthy. Foremost is Dr. Shu Namiki, my first labmate and one who has taught me much, from the physics of solitons and APM action to the aligning of an autocorrelator. His patience, careful listening, and encouragement are welcome to a young, eager graduate student making his way as an experimentalist. Dr. Moti Mordehai has been a welcome addition to the group–I've enjoyed our many arguments and debates over much of the work in this thesis, and I welcome his collegiate attitude. Dr. Gunter Steinmeyer has provided me with endless hours of assistance in the lab–I think that he wonders if there are any electrical engineers around here who–besides Siegfried F.–has a decent working knowledge of circuits.

There are many others whom I'd like to recognize, and apologies to those I have not explicitly mentioned here: Dr. Brett Bouma, who has patiently answered my many optics questions; Dr. Dominique Peter, I enjoyed working with her on a few projects and appreciate her direct manner and love of the outdoors; colleagues Charles Yu, Patrick Chou, and David Jones; the Fujimoto group of Igor, Boris, Steve, Gary, Seong-Ho, Costas and others; former students Dr. Luc Boivin, Dr. Lynn Nelson, Dr. Dave Doughtery and ever-the-unpredictable Dr. Siegfried Fleischer. Thanks to Dr. Masayuki Matsumoto, Dr. Stefano Longhi, and Dr. Franz Kärtner for helpful discussions. Thanks to William Wong for much helpful encouragement. I've enjoyed having Eric Thoen as an officemate, and his ready smile and sense of humor is always

welcome. Thanks to Dr. Reggie Brothers and Dr. Gerhard DeLonge for rf equipment advice and lending.

Thanks to all of my friends for their encouragement, including Kristina, Kris Joshi, Rahul Advani, Eric Simonson, and Paul Poirot.

There are many MIT faculty whom I must mention here: Prof. T. Orlando and Prof. J. Kong for their guidance as my course/area advisors. Thanks to Prof. Rajeev Ram for many impromptu discussions on quantum optics–I've learned much about semiconductor optics these last six months through our informal-but-engaging Saturday seminars.

I gratefully acknowledge the support of an NDSEG fellowship funded by the Department of Defense.

Thanks, too, for the encouragement from my former professors at Texas A&M University, including my previous advisor, Dr. Mark Weichold, who oversaw my two research projects as an undergraduate.

From Lincoln Labs, thanks to Dr. Katie Hall for providing much of the equipment used in this work. I appreciate her support and positive attitude, as well as her creative laboratory skills. Dr. John Moores has been very helpful in explaining some of his earlier work on the stabilization of solitons in a memory ring.

Thanks for the assistance of Donna Gale, Cindy Kopf, and Mary Aldridge–their professionalism and assistance really makes things work around here. Thanks to Eddie for late-night company.

Thanks to my family, including my twin brother Mark, older brother Stephen, sister Anne Claire and her husband Michael; and especially to my loving parents, whose support throughout my career has always been a mainstay.

> It is an old maxim of mine that when you have
> excluded the impossible, whatever remains,
> however improbable, must be the truth.
>
> Sherlock Holmes, *The Adventure of the Beryl Coronet*
> Sir Arthur Conan Doyle

Contents

List of Figures

List of Tables

Chapter 1

Introduction

In recent years, there has been substantial development in realization of all-optical communication networks with data rates of 100 Gbit/s and higher. Current trends have been pushing communication architectures in two directions: time-division multiplexing (TDM), a scheme that allows each bit stream to fill a reserved sequence of time slots; and wavelength-division multiplexing (WDM) in which bit streams are assigned different wavelength slots. Each has its advantages and disadvantages [45]. An ARPA-funded All-Optical Network Consortium (AON)–whose members include DEC, AT&T, MIT Lincoln Laboratories and MIT campus–has chosen a TDM architecture in the development of a 100 Gbit/s LAN/MAN (Local Area and Metropolitan Area Network) testbed. It is the stringent requirement of that architecture that sets the operation specifications for our laser development, listed in the next section.

1.1 Requirements of a TDM Source

- Repetition Rate
  - $f_{rep} = 10$ GHz
  - External control of repetition rate–we will need to synchronize multiple sources to multiplex up to the desired 100 Gb/s bit rate
  - Continuous operation at a fixed rep rate

- Pulsewidths τ = 1 - 3 ps; in TDM, shorter pulses increase the potential number of channels
- Tunability $\Delta\lambda$ = 10-20 nm around λ = 1550 nm
- rf sideband suppression > 60 dB; the pulse dropout rate can not exceed 10^{-6}

1.2 Active Modelocking

The action of the modelocker is to overcome the spectral narrowing of the gain medium by forcing oscillation in many phaselocked modes of the resonant cavity. With an amplitude modulator, this is achieved by periodically modulating the loss in the cavity at the round trip frequency. Pulses circulating in the cavity pass through the modulator when the loss is a minimum. The action of the modulator can be described by the transmission function

$$T = 1 - M(1 - \cos(\omega_m T)) \tag{1.1}$$

Physically, the modulator is an electro-optically controllable Mach-Zender interferometer. A voltage applied to one of the arms imparts a phase delay via the electrooptic effect, resulting in a voltage-dependent optical power output. By appropriately setting the bias of the interferometer with a dc voltage, the application of an rf voltage swings the transmission about some operating point. Typically, the modulator is operated in the linear regime, thus the set point is biased at an inflection point, shown schematically in figure 1-1.

The operating point on the sinusoidal transmission curve, Q_0, is set by the dc bias voltage applied to the modulator. To create the time-dependent transmission as in (1.1), we apply a time-varying signal $V_{rf}(\omega_m)$–here, a sinusoid with frequency ω_m. The applied voltage swings the transmission about Q_0, leading to a sinusoidally varying transmission as shown in the figure. V_π is the voltage required to switch the device on and off. M, the depth of modulation, is equal to one when the amplitude of the driving voltage, $V_{rf}(\omega_m)$, is equal to V_π. The time-varying transmission curve is

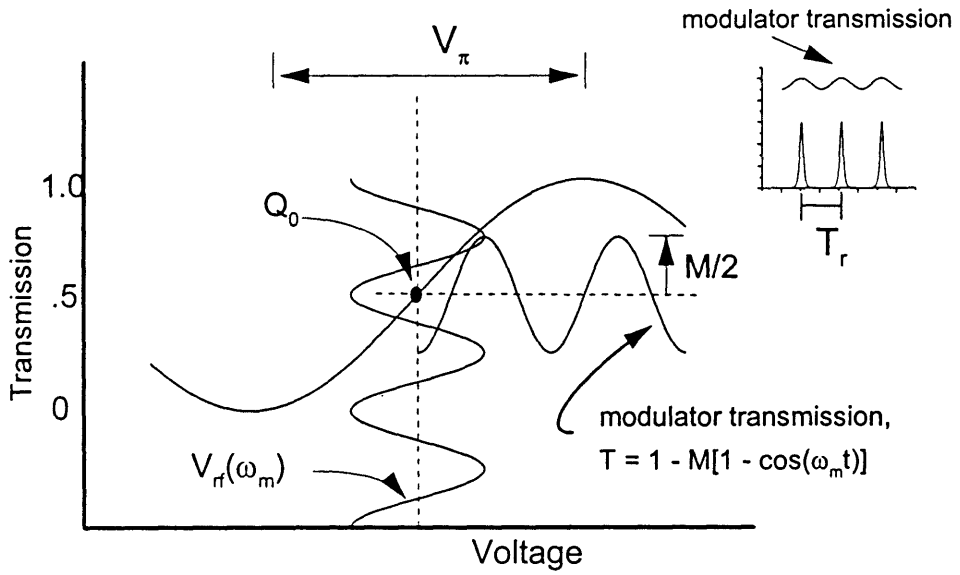

Figure 1-1: Modulator biasing scheme; Q_0 is the operating point set by the applied dc bias voltage, M is the modulation depth, V_π is the voltage required to swing the transmission function from a maximum to minimum, $V_{rf}(\omega_m)$ is the time-varying voltage applied to the modulator. The inset shows the resulting time-varying transmission function superimposed over the pulse train building up in a laser where the loss is minimum; T_r is the cavity round-trip time.

displayed in the inset of the figure with pulses superimposed on the time slots where the loss is a minimum, as occurs in the laser cavity.

We can write the combined effects of modulation, gain, and linear loss in the formalism of the master equation [20] as

$$T_R \frac{\partial a(T,t)}{\partial T} = -iD\frac{\partial^2}{\partial t^2}a(T,t) + \left\{ g\left(1 + \frac{1}{\Omega_g^2}\frac{\partial^2}{\partial t^2}\right) - l - M_{AM}[1-\cos(\omega_m t)] \right\} a(T,t) \tag{1.2}$$

In the above, we have written the evolution of the envelope of the electric field a with respect to two time scales: T, on the order of the roundtrip time, and t, on the order of the pulse width. Too, we have included the effects of linear group velocy dispersion (GVD) D, where $D > 0$ is normal dispersion (group velocity increases with increasing wavelength), and $D < 0$ is anomalous dispersion (group velocity decreases with wavelength). Setting the LHS to zero is the condition in which the modulation frequency is set to equal the cavity oscillation frequency: $\omega_m = \omega_c$. Assuming that the pulse for our solution is much shorter than the round trip time (usually picoseconds versus nanoseconds, a thousand times shorter), and assuming that the pulse will arrive at the modulator where it experiences the least loss, we can expand our modulation function as a Taylor series: $M[1-cos(\omega_m t)] \approx -M\frac{\omega_m^2 t^2}{2}$ and the eigensolutions for the resulting linear partial differential equation become the family of Hermite-Gaussians. It turns out that the lowest order eigenmode with $n = 0$ is the most stable; that is, it experiences the highest gain per round trip [19], so our solution becomes

$$a(t) = a_0 \exp\left(-\frac{t^2}{2\tau_a^2}\right) \tag{1.3}$$

where τ_a is the pulse width of the Gaussian given as

$$\tau_a = Re\left\{ \sqrt[4]{\frac{D_g - jD}{M_{am}}} \right\} \tag{1.4}$$

where

$$D_g = \frac{g_0}{\Omega_g^2} \tag{1.5}$$

$$M_{am} = \frac{1}{2}M\omega_m^2 \tag{1.6}$$

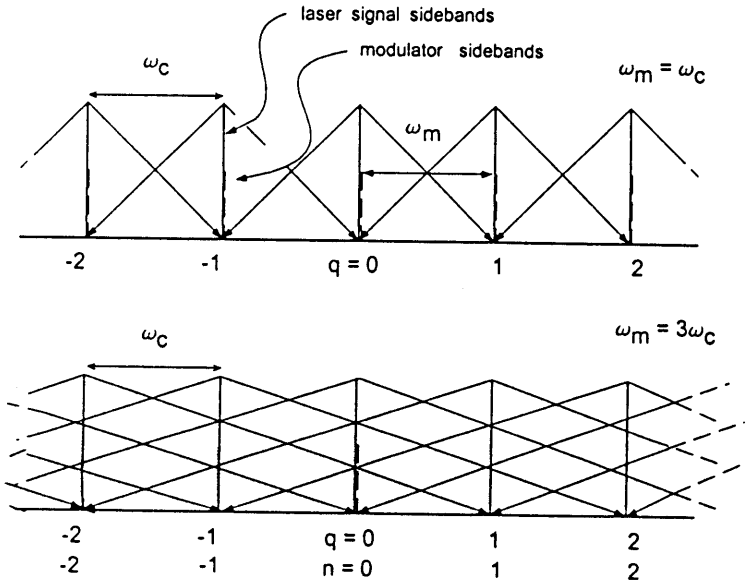

Figure 1-2: Supermodes in the frequency domain

The effect of group velocity dispersion D broadens the pulse in the time domain, regardless of its sign.

Note that the above solution is a steady-state analysis–we have not considered how long it takes the modulator to bring the modes into synchronism. Siegman [43] found that a strongly homogeneously-broadened gain laser initially oscillating in a single mode takes N_{ss} round trips to converge to the final steady-state solution above, where $N_{ss} \approx \Omega_g/\omega_m$. For typical erbium fiber lasers, we can take $\Omega_g \approx 40$ nm, and for $\omega_m = 2\pi \cdot 10$ GHz, we find $N_{ss} \approx 500$ round trips.

1.3 Harmonic Modelocking

At the repetition rates of GHz we are interested in, a corresponding cavity would need to be on the order of centimeters, clearly impractical for our laser due to the minimum amount of erbium-doped fiber needed for gain. The erbium doping level in the silica host is limited due to unavoidable atomic clustering effects [10]. Too, the amplitude modulator alone is at least 10 cm long. Thus, the modelocking frequency ω_m will be some harmonic of the fundamental such that $\omega_m = N \cdot \omega_c$. In the time domain, this implies that there are now N pulses in the cavity rather then just one. The

above equations remain unchanged; however, there is a qualitative difference in the modelocked laser operation; namely, there will be a new noise source not encountered for the N = 1 case, perhaps best viewed in the frequency domain, shown schematically in figure 1-2. The modulator creates sidebands separated by $\omega_m = N \cdot \omega_c$, and these sidebands phaselock the overlapping cavity modes. The q's denote the laser signal sidebands, shown with solid lines. The dotted lines represent the modulator signal sidebands. For the single harmonic case, the modulator injection-locks each of the laser signal modes with each other. For the N=3 case, the modulator injection locks laser signal sideband q with q $\pm$ 3. For instance, the n = 0 is the family of modes q = ...-6, -3, 0, 3, 6, ... There is another family of modes n = 1 that is spaced just ω_c away with members q = ...-7, -4, -1, 2, 5, ..., and this family bears no phase relationship with the other n families–these are the supermodes [19] that will compete for gain and cause amplitude fluctuations in the laser output.

The mode competition effects can be complicated if the involved modes have weak amplitudes. In such a case, quantum-limited noise incoherently dumping photons into random modes can swing the competition from one mode to the next. If 1 mode dominates, then one gets N pulses/period; for > 1 mode, there may be anything from 1 pulse to N pulses/period, depending on the relative phases. The extent of mode competition is a strong function of both the actual curvature of the gain spectrum and extent of homogeneous or inhomogeneous broadening. The degree of homogeneous versus inhomogeneous linewidth broadening is an important issue when considering the dynamics of supermode competition in the general case, but erbium-doped silica can be considered dominantly homogeneous [50] [4].

1.4 Previous Work

The shortest pulses are usually generated with passive modelocking techniques wherein one does not actively drive a modulator to phaselock the cavity modes; rather, the pulse induces its own shortening [25]. There have been some reported successes with passively modelocked systems invoking a sub-ring for repetition rate control [49,

(September 1991)] and generating femtosecond pulses; however, the pulse-to-pulse energy fluctuations could not be stabilized. An interesting technique demonstrated by Greer and Kimura et al [14, (August 1994)] utilizing cross-phase modulation could generate a stable stream of 1.2 ps at ten GHz; however, that technique relied on an external source of an already stable modelocked stream of pulses. S. Gray and A.B. Grudinin et al [13, (May 1994)] have showed the extremely low timing jitter of a harmonic passively modelocked laser at roughly 500 MHz. The ring was reportedly stabilized by the long-range soliton interaction driven by transverse acoustic wave excitation from the pulse-induced electrostriction in the fiber produces small changes of the refractive index, with δn on the order of 1 part in 10^{11} to 10^{13} [15]. While this solution is fortuitous and rather simple, it is not inherently clear that the technique could lend itself to GHz operation with dynamic control of the repetition rate.

So, passive modelockers have not yet demonstrated stability in generating multiple pulses per pass, and high repetition rates from a single pulse per pass laser cavity are impractical. There has been some interesting work on short-cavity, passively modelocked lasers that have generated sub-picosecond pulses at rates of up to 500 MHz, but the prospects for extending that up to GHz and beyond are far from clear.

Numerous groups have built active, harmonically modelocked lasers featuring high repetition rates and short pulses: A. Takada, H. Miyazawa [46, (December 1989)] 7.6 ps at 30 GHz, time-bandwidth product (TBP) of 0.47[1], H. Takara, S. Kawanishi, et al [47, (September 1992)] 3.5 - 10 ps at 2-20 GHz, TBP of .31 - .33[2]; and Th. Pfeiffer, G. Veith [39, (August 1993)] $<$ 6 ps at 40 GHz, TBP of .44 for a Gaussian pulse.

While impressive, none of these systems can be used in a communications systems without stabilization. Recall that the role of the modulator is to create a set of sidebands overlapping the cavity modes. Via injection locking, these cavity modes become coupled and phaselocked. As the cavity length changes via thermal or mechanical vibrations, the cavity longitudinal mode spacing changes since $\omega_c = c/nl$, where nl is the optical cavity length. When the difference between the modulation

[1]Gaussian pulse transform-limited TBP is .441

[2]sech pulse transform-limited TBP is 0.315

frequency and cavity mode spacing becomes too large for the modulator to pull the modes into synchronism, modelocking is lost and the pulse disintegrates.

So far, we have discussed techniques for generating pulses directly from a fiber laser. One of the dominant–and simplest–methods of generating a high rep-rate bit stream is the production of gain-switched pulsed from a semiconductor laser diode (SLD) . The fast gain recovery–on the order of picoseconds–makes such modelocking techniques possible. By injection seeding with external cw tunable light sources, some groups have achieved large tunability [5] [31] [8] [3] and reduction of pulse-to-pulse timing jitter [40]. Reports of gain-switched SLD's have achieved in excess of 40 nm of tuning at 11 GHz modulation [3] and 20 nm of tuning at 12 GHz [5]. While the repetition rate of these structures is limited by the available bandwidth of the SLD's to around 10 GHz, some faster Fabry-Perot (FP) multiple-quantum-well (MQW) lasers have recently been reported with bandwidths exceeding 28 GHz [33]. One of the major drawbacks is that the pulses typically emerge as long (5-7 ps) and highly chirped, requiring optical compression techniques to arrive at nearly transform-limited shapes [1].

Another approach is externally modulating the output of a cw semiconductor laser [30]. It has been shown that transform-limited pulses can, in fact, be generated with the appropriate use of a phase modulator and spectral filtering [32] or with an electroabsorption modulator (EAM) with a sinusoidally varying bias [44] [6]. But even then, the pulses are rather long (tens of picoseconds pulsewidths).

In comparison with direct and external modulation of SLD's, the output pulse quality directly from the fiber laser is good–typically near transform limited and requires no external compensation.

1.5 Detuning

One can make a rough estimate of the allowable detuning [43] as

$$|\delta T| = \frac{|\delta\omega_d|}{\omega_{AM}^2} \ll \frac{\tau_a}{N_{ss}} \tag{1.7}$$

where N_{ss} is the number of round trips required for the laser to form a steady-state pulsewidth from an arbitrary input state, and τ_a was given previously. The resulting is that the cavity must be stabilized within tens of kilohertz to maintain modelocking. Eqivalently, the length of the cavity would need to be stabilized to within $\Delta L/L = \Delta\omega/\omega \approx 1 \times 10^{-6}$ to 10^{-7}, or 5-50 μm for a 50 meter cavity. The dominant environment perturbation is thermal; that is, the index of refraction varies with temperature T. The optical path length varies as $L = L(n + \partial n/\partial T \Delta T)$, so the equivalent requirement for thermal stability is within 1×10^{-2} of a degree C.

1.6 Stability Techniques

Various schemes have employed feedback loops to compensate for environmental perturbations: Harvey and Mollenauer [16] employed a high-finesse étalon with a free spectral range equal to the cold-cavity repetition rate to generate an error signal to detect detuning. The scheme requires tailored tuning elements, and, because of the possibility that two adjacent supermodes symmetric about the étalon peak could result in unstable mode beating, some mechanism enforcing active stabilization of the ring length via fiber heating or piezoelectric mirror movement was employed. Wey and others [48] improved on this scheme by incorporating a complicated phase-locking circuit to match the étalon transmission peaks with the cavity modes and applying a dithering signal to prevent random symmetric supermode competition. Shan, Cleland, and Ellis [41] employed a PZT-based length compensator to match environmental detuning effects; however, while error-free operation up to two Gbit/s was demonstrated, such a mechanical compensation technique will suffer from environmental degradation. While the previously mentioned paper of H. Takara and S. Kawanishi et al [47], has reported error-free operation at both four and eight Gbit/s using polarization-preserving fiber in the cavity to stabilize the polarization of the cavity modes, it is not clear that such a method will be stable enough without compensating for detuning as temperature fluctuations and/or mechanical vibrations carry the cavity mode spacing away from the modulator drive. In a later work, Shan and

Spirit [42] implemented a kHz dither to the piezoelectric drive to suppress supermode competition, achieving error-free operation for one-hundred minutes at 2.5 Gbit/s, but longer term stability on the order of hours is a key requirement for a useful source. A scheme by Nakazawa [35] employs a regenerative modelocking scheme to modify the modulator drive to follow the changing cavity mode spacing in a fashion similar to techniques first employed to other laser systems [23] [28] [7]. While no bit error rates have been reported, this system was recently observed to have achieved long-term, error-free operation [24]. The regenerative modelocker is an attractive solution for achieving long-term stability and one that was chosen for further investigation in this thesis.

1.7 Optical Solitons

Since the earliest predictions of soliton effects in optical fibers [17], the soliton has received much attention for exhibiting some rather remarkable properties, most importantly for pulse propagation without chromatic or temporal distortion. While solitons exhibit a variety of interesting phenomena worthy of intense study, only a cursory review will be given here to illustrate the most relevant properties.

The master equation governing the evolution of the electric field in an optical fiber can be written as a nonlinear Schrödinger Equation (NLSE)

$$\frac{\partial}{\partial z}a(z,t) = -i\frac{1}{2}\beta''\frac{\partial^2}{\partial t^2}a + i\delta|a|^2 a \tag{1.8}$$

where a(z,t) is the electric field amplitude, β'' is the dispersion, and δ is the self-phase modulation (SPM) coefficient. Notice that our term for dispersion here, β'', is related to our previous term D as

$$\beta'' \equiv \frac{\partial}{\partial\omega}\left(\frac{1}{v_g}\right); \tag{1.9}$$

$$D \equiv \frac{\partial}{\partial\lambda}\left(\frac{1}{v_g}\right); \tag{1.10}$$

$$D = -\frac{2\pi c}{\lambda^2}\beta'' \tag{1.11}$$

where v_g is the group velocity of the electric field amplitude. We have written (1.8)in a reference frame moving with the pulse (i.e, t=0 is the pulse center). a(z,t) is normalized such that the pulse energy is given by $W_s = \int a^* a \, dt$. The lowest-order solution to the above takes the form

$$a_s(z,t) = \sqrt{P_s} sech\left(\frac{t}{\tau}\right) \exp(j\frac{1}{2}k_s z) \tag{1.12}$$

where P_s is the peak power, and ϕ_s is the nonlinear phase shift where

$$\phi_s = \frac{1}{2}k_s z = \frac{1}{2}\delta P_s z \tag{1.13}$$

We can define a length scale by the soliton period by

$$z_0 \equiv \frac{\pi}{4}\frac{\tau^2}{\beta''} \tag{1.14}$$

such than in a propagation distance z_0, the fundamental soliton accumulates a phase shift of $\pi/4$. Smaller dispersion and larger pulsewidths lead to a larger period. It can be shown that the NLSE obeys an area theorem coupling the width τ_s to the intensity:

$$W_s\tau = 2P_s\tau^2 = 2\frac{\beta''}{\delta} \tag{1.15}$$

1.8 Overview of the rest of the Thesis

It turns out that solitons in fiber lasers are only quasi-stable and, under the influence of periodic perturbations, must be stabilized. In chapter two, we discuss the relevant issues needed to stabilize the soliton in the actively modelocked laser and derive stability criteria. In chapter three, we present the results from active modelocking without stabilization (AML) and identify the limits of long-term stability. Then in chapter four, we describe the regenerative modelocking (RML) scheme, derive governing equations for the feedback, and compare its operation with AML. In chapter five, a brief summary is given along with a plan for future work. The clock extraction hardware used for the regenerative scheme is described in appendix A. In appendix B, the chirp imposed on the optical signal as a function of the dc voltage applied to the modulator is derived. In appendix C, details on dispersion measurements are presented.

Chapter 2

Active Modelocking and Solitons

2.1 Soliton Formation

In the introduction, we reviewed active modelocking by loss modulation with an electrooptic modulator and found an analytical expression for the resulting pulsewidth, τ_a, as

$$\tau_a = Re\left\{\sqrt[4]{\frac{D_g - jD}{M_{am}}}\right\} \tag{2.1}$$

So, for $\omega_m = 10$ GHz, $\Omega_g = 30$ nm (i.e., just gain filtering) we find that the resulting pulsewidth, ignoring dispersion, is approximately 5 picoseconds for $D = 0$. And including dispersion only broadens the pulse. In our list of requirements, we wanted 1-3 ps, so what can be done?

Haus and Silberberg [22] showed that the addition of a nonlinear index can, by means of spectral broadening via SPM, assist the active (or passive) modelocking process in overcoming the spectral limiting action of gain dispersion to achieve a reduction in pulsewidth by a factor of 2.5. Further reduction leads to the onset of instability, a signature characterized by oscillations in the pulse shape and pulse energy. Kärtner et al. [26] later showed that, with the addition of strong anomalous dispersion, soliton formation can be achieved with pulsewidth reductions greater than 2.5, given by

$$R < \frac{1.66}{1.76}\sqrt[4]{\frac{9}{2}\frac{|D|}{D_g}} \tag{2.2}$$

Arbitrarily increasing the amount of anomalous GVD does not allow us to get an arbitrarily large value of R, as explained in more detail below–the formation of the soliton comes with the cost of the accompanying continuum.

2.2 Soliton Stability and Continuum Suppression

As shown by Gordon [12], perturbations to the soliton result in the soliton shedding energy into the continuum. For the soliton, SPM and GVD stay in balance, thus the soliton preserves its shape; the continuum, however, does not experience SPM, becomes broadened by GVD, and thus sees higher loss in the modulator than the soliton. However, compared to the continuum, the spectrally broad soliton sees more loss from filtering. The soliton will be stable as long as the continuum sees less round-trip gain than the soliton. Thus, there is balance between the amount of GVD, strength of modulation, and filtering strength needed to support solitons in an actively modelocked system.

From the perturbation theory, we find that the condition [21] for the gain to be greater than any competing noise source is given by

$$\frac{\pi^2}{24} M\omega_m^2 \tau^2 + \frac{1}{3}\frac{1}{\Omega_f^2 \tau^2} < Re\left[\frac{1}{2} M\omega_m^2 \left(\frac{1}{\Omega_f^2} - \frac{1}{2} j\beta''\right)\right]^{\frac{1}{2}} \tag{2.3}$$

We need to ensure that fluctuations in the soliton energy are also suppressed, resulting in

$$\frac{\pi^2}{24} M\omega_m^2 \tau^2 - \frac{1}{3}\frac{1}{\Omega_f^2 \tau^2} < 0 \tag{2.4}$$

Figure 2-1 shows the region where the conditions in equations 2.3 and 2.4 are satisfied. [1] The maximum reduction in pulsewidth within the stability criteria above is given by [26]

$$R_{max} = \frac{1.66}{1.76} \sqrt[12]{\left(\frac{9}{2}\phi_{nl}\right)^2 \frac{1}{D_g}} \tag{2.5}$$

[1] Note that in comparison with the figure shown in reference [21], both of the axes here are scaled down by a factor of two.

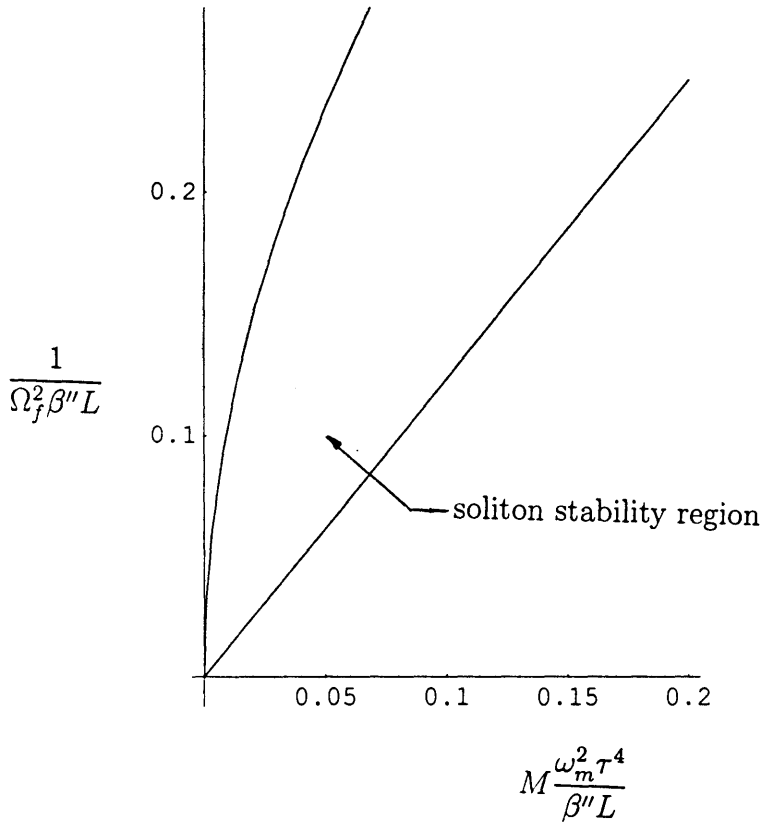

Figure 2-1: Region of stability permitting the growth of solitons at the expense of the continuum

Chapter 3

Active Modelocking Experiments

3.1 Experimental Setup

Figure 3-1 shows the experimental setup. The displayed "switch" is actually a set of fiber splitters/combiners of varying ratios allowing us to choose how much power of the output to peel off for clock extraction, with the rest going to the "monitor", an array of diagnostic equipment including the rf spectrum analyzer, optical spectrum analyzer, power meter, and autocorrelator (non-collinear type). The fiber in the cavity is all polarization maintaining (PM), including the 980 nm/1550 nm wave-division multiplexer (WDM) and output couplers. The modulator is an AT&T Mach-Zender type 2122AA $LiNbO_3$ with a titanium indiffused waveguide with an rf input impedance of 43 Ohms, and the optical insertion loss exceeds 4 dB. The optical filters used in the setup are interference type and angle tunable from 1560 nm down through the entire erbium gain spectrum. Across the air gap, the optical field is both launched and refocused by aspheric lenses mated to PM fiber pigtails–coupling across the air gap is on the order of 70 %. The role of the $\lambda/2$ waveplate is to map the linearly polarized electric field emerging from the left aspheric lens to the right. The isolator is polarization sensitive and aligned to the fiber's slow axis, as are the modulator and other components, and imparts 1 dB insertion loss. The role of the polarization-sensitive isolator is threefold: first, it ensures unidirectional lasing direction in the CW direction by breaking the degeneracy with the equally-probable

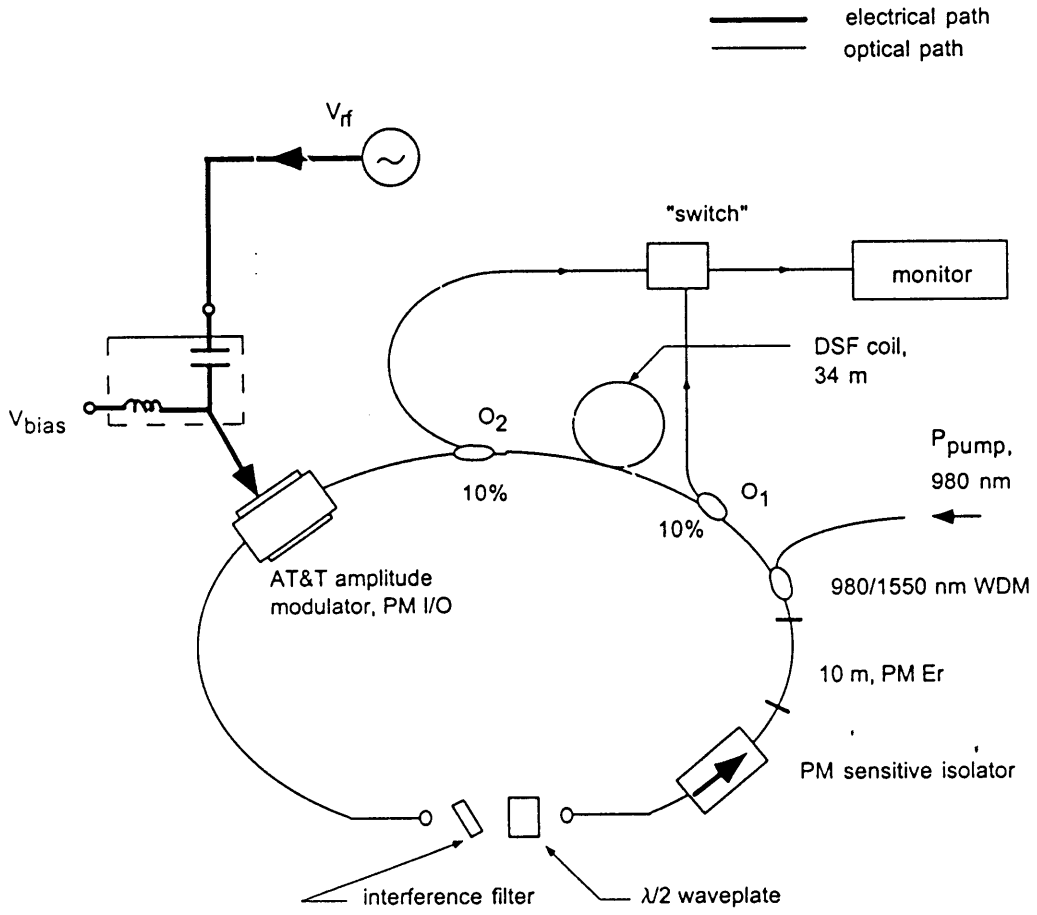

Figure 3-1: Experimental setup for AML

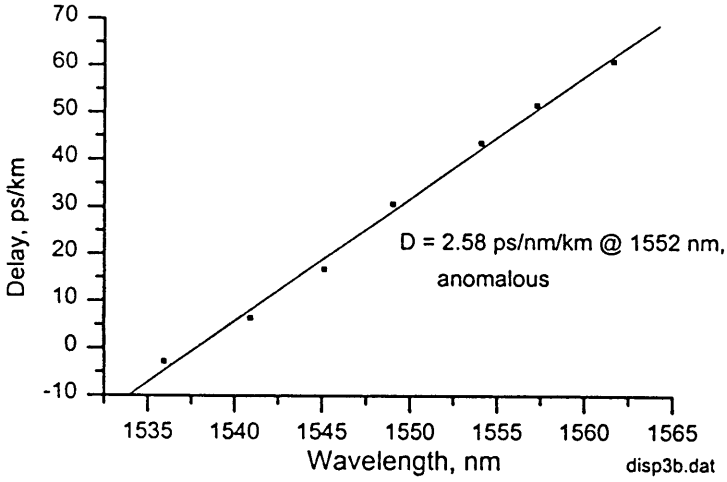

Figure 3-2: Delay as a function of wavelength. The positive slope indicating increasing delay with wavelength corresponds to anomalous dispersion.

CCW longitudinal modes. Second, because it is sensitive to the input polarization, we can ensure that the waveplate is properly set by monitoring the output power–any misalignment of the waveplate results in linear loss. Third, with its placement just before the Er fiber, it ensures that none of the CCW propagating 980 nm pump light reaches the amplitude modulator–an important consideration, given that the $LiNbO_3$ tends to absorb in that wavelength region, resulting in photorefractive damage for 980 nm light levels on the order of a few milliwatts. Measurements just after the waveplate (looking to the right, into the Er fiber) with a sensitive power detector (range to -60 dBm) yielded 980 nm pump power on the order of nanowatts. 10 meters of Er fiber ($\beta'' \approx +10 \text{ps}^2/\text{km}$) follows the isolator, then the WDM, output coupler O1, spool of dispersion-shifted fiber ($\beta'' \approx -2.5 \text{ps}^2/\text{km}$), then output coupler O2.

The dispersion for the loop was measured by two different techniques: the first method is similar to that given by Knox [29] in which the group velocity delay is measured as a function of wavelength, displayed in figure 3-2–for further discussion, see Appendix C. The second method was based on the position of the sidebands and the soliton pulsewidth [9] when the laser was modelocked. The two methods were in good agreement: the first method gave + 2.58 ps/nm/km, and the second + 2.60

ps/nm/km.

The role of the 34 m DSF loop is twofold: first, the shifted dispersion allows us to bring down the average intracavity dispersion; that is, to make the average less anomalous. The required intracavity power needed to support solitons in a system with average dispersion β'' at repetition rate R with pulsewidth τ_s requires that

$$P_{av} > 1.4\frac{\beta''}{\tau_s}R \tag{3.1}$$

where β'' is in ps^2/km, R in GHz, τ_s is the full-width-at-half-maximum (fwhm) pulsewidth in ps, and P_{av} in mW. This is, at best, a lower limit on the amount of intracavity power necessary since the pulses will shed a significant portion of their energy to the continuum. For a 10 GHz pulse train of 1 ps pulses and $\beta''_{av} = 3$ ps^2/km, the required intracavity power is > 42 mW. In our system, the available intracavity power is on the order of 80 mW. The second role of the long DSF loop is in the generation of excess SPM to aid in soliton compression and supermode suppression (discussed in more detail in a following section). The important point here is that one would like the highest amount of intracavity power in the DSF portion of the laser–it is here that the splicing issue becomes relevant.

The dispersion in optical fiber is composed of two parts: material and waveguide dispersion. The waveguide dispersion can be manipulated to shift out the zero-dispersion wavelength from 1.3 μm in typical fiber toward 1.5 μm in DSF. This, unfortunately, results in a large mismatch between the waveguiding cores between DSF and non-DSF fiber. The mode-field mismatch between DSF and non-DSF is about 3 μm and results in splice losses between 20% and 25%–around 1 dB–when typical methods used to splice identical fibers are employed. We were able to reduce the loss to 8%, at best, by utilizing techniques documented elsewhere [1]. We have suggested other techniques to further improve the reduction in splice loss to approximately 4-5%, but that effort is beyond the scope of this work–8% is an acceptable figure here.

The output power from ports O1 and O2 with 350 mW pump at 980 nm yielded

[1]RLE internal document, MIT, to be published

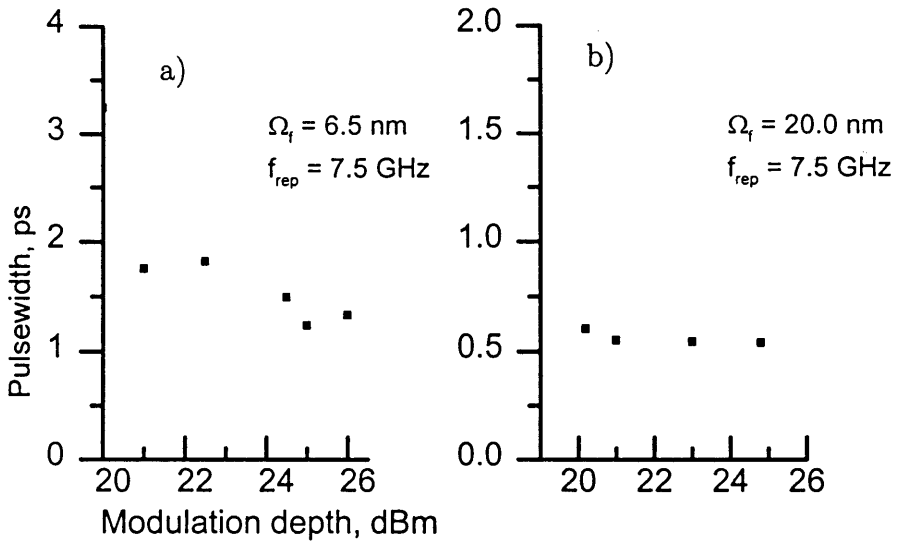

Figure 3-3: Measured fwhm pulsewidth as a function of modulation strength. The modulation frequency here is 7.5 GHz, and the filter strength for case a) is 6.5 nm, and for case b) is 20 nm. Notice that the τ axis in b) is scaled to 1/2 of that in a)

8.0 and 2.9 mW, respectively. Estimating the combined loss for the two DSF splices as 20 % still leaves another 3 dB of loss unaccounted for. We can relate the pulses from O2 to O1 by the dispersive broadening in the 34 m DSF link with dispersion + 2.5 ps/nm/km between the output ports. Ignoring SPM effects, a 1 ps pulse will broaden by 210 fs, a change of 20 %. SPM effects will, instead, shorten the pulse depending on pulse energy–we measured that a 602 fs pulse at O1 yields a 460 fs pulse at O2, yielding a 26 % difference. In the results below, the pulsewidths and optical spectra are taken from port O1, so our reported figures for the minimum pulsewidth are conservative.

3.2 Experiments

The optimum operation of the laser is one that yields the shortest pulses while suppressing pulse-to-pulse amplitude fluctuations. So, the two issues here are:

- We will need to clean up the shed continuum created by soliton formation. Assisting us in finding the appropriate parameters (i.e., dispersion, filtering

strength, modulation strength) is the analysis of chapter two, graphically displayed in figure 2-1. The shortest pulsewidths are achieved for the largest modulation strength and weakest filtering. Even though both axes scale inversely with dispersion, we know from chapter one that τ scales roughly as the square root of dispersion, so the x-axis will roughly scale as:

$$\frac{\tau_s^4}{\beta'' l} \approx \beta'' l \tag{3.2}$$

Thus, an increase in total dispersion moves down on the y-axis and to the right on the x-axis, requiring either a small increase in filtering or decrease in the modulation strength. Once soliton effects begin to shorten the pulse, the action of the modulator is of first order in continuum cleanup and retiming, and of second order in pulse shaping. Figure 3-3 displays characteristics of the pulsewidth decreasing with modulation strength using the 6.5 and 20 nm filters. We can see that for the smaller filter, the pulses are rather large–on the order of 1.5 to 2 ps–and increasing the modulation depth beneficially reduces the pulsewidth. In case b), the pulses are much shorter, and the modulator is much less effective in pulse shaping.

Note that the data in the figure was recorded for a slightly modified configuration than that of our setup as described in figure 3-1; namely, a different Er fiber and different type of amplitude modulator was employed, and the modulation frequency here is 7.5 GHz rather than 10 GHz; however, the point here is a qualitative one and holds for both configurations.

- We need to ensure that we have pulses in every time slot, not just a single, very short soliton in a single time slot–this issue is discussed in more detail in a later section. We can estimate the effectiveness of pulse quantization by looking for pulse dropouts and amplitude modulations in the rf spectrum by the suppression of the supermodes. For example, consider a cavity with a fundamental repetition rate of 10 MHz operating at 10 GHz. Then, at any given time, there exists a pulse train of 1000 pulses inside the cavity circulating at the rate of 10 MHz–that is, the pulse pattern repeats every 10 MHz. If all

1000 pulses had equal amplitude, then a single Fourier component of the pulse train would show up on the spectrum analyzer (including harmonics of 20, 30, 40 GHz, etc...), and the sidebands would be below detection. If one pulse out of 1000 were missing, or if there were a 1/10 of 1 % amplitude fluctuations on the pulse train at the cavity repetition rate, then the intensity of the sidemodes would be 1 part out of 1000 of the main Fourier component at 10 GHz, thus -30 dB down. The fundamental cavity frequency was 3.667 MHz, so there are 2727 pulses in the cavity we investigated at 10 GHz. A single pulse dropout (or amplitude modulation of $1/2727 = 0.03$ %) will show up in the rf spectrum as sidebands spaced at the fundamental cavity frequency $\omega_c = 3.67$ MHz that are -34 dB down from the main Fourier spectral component at 10 GHz.

In all of the experimental results below, the amplitude modulator was biased at the 3-dB point and operated in push-pull mode. The frequency of the signal generator driving the modulator was adjusted until the rf signal $V_{rf}(\omega_m)$ was equal to a cavity harmonic around 10 GHz. The onset of modelocking was monitored with both an rf spectrum analyzer (bandwidth of 22 GHz) and an optical spectrum analyzer.

3.3 Experimental Results and Analysis

While we did not explore the entire parameter space, we know that the optical filter plays an important role: 1) it sets the lasing wavelength and allows for wavelength tunability, 2) it is the strongest spectral filter in the cavity and, in conjunction with dispersion and amplitude modulation, plays an important role in continuum cleanup, and 3) with SPM, helps to induce spectral loss, as discussed in another section, that contributes to pulse-to-pulse stability. Keeping P_{pump} constant, we inserted filters of varying optical strength and monitored the change in pulsewidth, optical spectrum, and rf spectrum.

A typical trace with the 20 nm optical filter is given in figure 3-4. The pulsewidth is 840 fs, the center frequency is 1552 nm, the intracavity power is approximately 8.0 mW, and the pulse energies are 800 fJ/pulse. With an intracavity dispersion

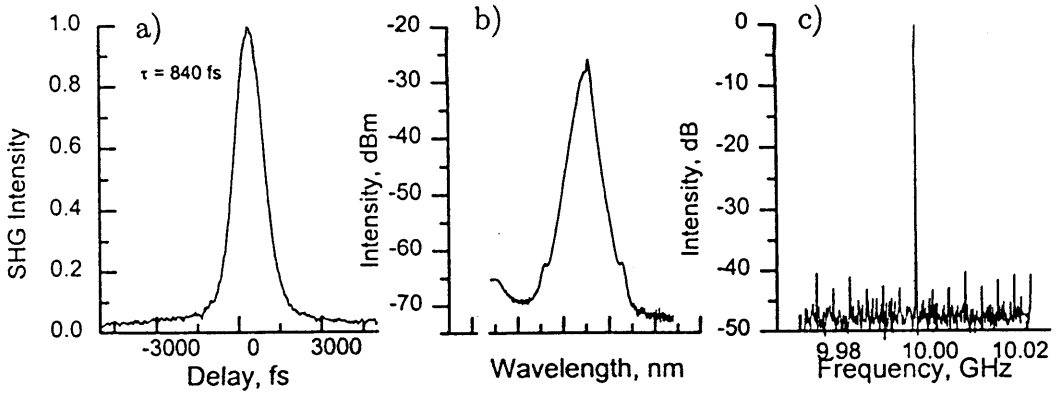

Figure 3-4: Typical lasing characteristics of the AML. The filter bandwidth for the above results was 20 nm; a) autocorrelation, $\tau_s = 840$ fs is the fwhm value fit to $sech^2$ b) optical spectrum, c)rf spectrum, 50 MHz span

of 3.2 ps^2/km, the minimum amount of intracavity power needed to support τ_s is $P_{av} > 50/\tau_s$. With 8.0 mW at the output coupler, that gives 80 mW internally, enough to support a 10 GHz train of 600 fs pulses. The sidebands at $\pm$10.2 nm in the optical spectrum are explained by Kelly et al. [27], where the shed continuum and soliton, traveling with different group velocities, become phase matched. This issue is an important one and discussed in more detail below. The rather small optical sideband amplitudes in the figure suggest that the continuum sees large losses and is effectively cleaned up by the action of the modulator, dispersion, and optical filtering.

For a given filter strength, the operating conditions for the AML case were found by varying the modulation strength and driving frequency until the laser was modelocked with the best supermode suppression. Varying the modulation strength by 2-3 dB had a very weak effect on the pulsewidth, as expected, but for much smaller or much larger modulation strengths, we observed a growth in the continuum accompanying the pulse that could be seen in the autocorrelation traces. We can attribute the continuum accompanying the pulse in the autocorrelation trace in figure 3-4 to the cw background also observed in the optical spectrum. While tuning the lasing

filter, nm	τ^{fwhm}, ps	$\Delta\lambda$, nm	rf , dB	$\Delta\lambda_s/\Delta\lambda_f$	ϕ_{nl}, radians	R_{meas}
2.5	4.2	0.6	30 ± 2	24 %	.016	1.4
6.5	1.0	2.5	40 ± 2	38 %	.29	3.5
20	.602	4.2	45 ± 2	21 %	.80	3.3

Table 3.1: Active modelocking results with varying filter strength

frequency across the erbium bandwidth, we found that the spectral position of the cw remained relatively constant with respect to the pulse spectrum.

The rf spectrum in figure 3-4 shows sidemode suppression below -40 dB, indicating that there are no pulse dropouts and a small amplitude modulation on the order of 1/100th of 1%.

The results for filter strength of 2.5, 6.5, and 20 nm are compiled in table 3.1. For each measurement, the laser was stable for five to ten minutes, and the onset of instability could be monitored via the rf spectrum–the supermodes grew rapidly, and the autocorrelation level decreased (maximum level of the autocorrelation signal monitored), thus indicating a drop in peak power. The laser could be kept stable as long as one made slight adjustments to both the modulation frequency and modulator bias voltage.

In the table, R_{meas} is defined as before–the ratio of the pulsewidth expected without nonlinear shaping effects versus the measured pulsewidth. $\Delta\lambda_s$ is the fwhm of the pulse spectrum, and $\Delta\lambda_f$ is the fwhm of the filter transmission. The values reported here are consistent with those predicted by the theory of Kärtner et al [26], reviewed in the previous section, except for the R = 3.3 value for the 600 fs pulse. R scales with the square root of the filter bandwidth, so increasing from the 6.5 to 20 nm filter should have given an increase in $\sqrt{20/6.5} = 1.8$, giving an R of at least 6.1. There is a fundamental limit to R_{max} not accounted for in equation (2.5) that is given by the resonant instability inherent in soliton fiber lasers, described below.

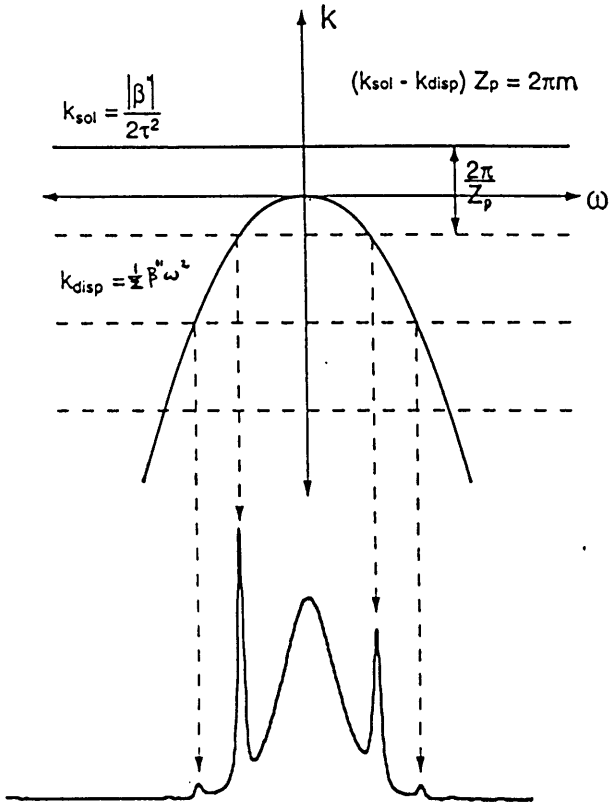

Figure 3-5: Phase-matching condition and Kelly sidebands

3.4 Soliton Sideband Generation

In chapter two, we discussed the controls of filtering, modulation, and dispersion needed to suppress the continuum generated by the soliton. The continuum travels as a linearly propagating dispersive wave [18] that is initially shed with the same phase as the soliton, but each frequency component then travels at the phase velocity of the medium. The dispersive waves are generated every round trip with period z_c, the length of the cavity. Where the differential phase shift between the soliton and the dispersive waves is a multiple of 2π, the interference between them is constructive, giving rise to sidebands in the soliton spectrum, as shown in figure 3-5. These are the so-called Kelly sidebands [27] [11] [12] [38]. The phase matching condition is met where

$$\Delta\omega_N = \pm\frac{1}{\tau_s}\sqrt{\frac{z_0}{z_c}8N - 1} \tag{3.3}$$

where $\Delta\omega_N$ is measured from the center of the soliton spectrum; N is the sideband order, where N = 1, 2, ..., counting from the center of the pulse spectrum; and z_0

is the soliton period, defined in chapter one, as the distance over which the soliton acquires a phase shift of $\pi/4$. As τ_s decreases, z_0 decreases, and the sidebands move in closer to the center of the spectrum. Notice that when the cavity length z_c approaches the soliton period, the sidebands occur at the center of the pulse–this situation corresponds to the pulse acquiring a nonlinear phase shift $\phi_{nl} = 2\pi$. The pulse can never actually become this short, and previous studies have shown that ϕ_{nl} can be only as be as large as $3\pi/8$. Thus, the pulse shortening is said to be sideband limited.

From the table, we see that $\phi_{nl} = .8 = 2\pi/8$; thus, it may be that our pulse is, in fact, close to sideband limited.

The results show that the shortest pulses with the best supermode suppression are obtained with the 20 nm filter, suggesting that the mechanism responsible for stabilizing pulse-to-pulse amplitude fluctuations is one that presents shorter pulses with greater loss (spectral limiting). The sideband-limiting described above describes one such mechanism: an increase in photon number can not help in shortening the pulse and scatter into the continuum, thus providing a mechanism preventing a single, very short pulse at the expense of the other time slots. In the following section, we suggest two other possible mechanisms that may also be at work: SPM + filtering, and modulator-induced loss.

3.5 SPM + filtering

One mechanism giving rise to increasing loss for a shorter pulse is given by the action of filtering and SPM. Consider a simple, second-order bandpass filter given by F(ω). The transmission through the filter is given by

$$|F(\omega)|^2 = \frac{\omega^2}{\omega^2 + \left(\frac{\omega^2 - \omega_0^2}{\Delta\omega_f}\right)^2} \tag{3.4}$$

Filter loss, $\text{loss}_{filter}(\tau_s)$, is given as the product of the pulse spectrum with the amplitude filter function, integrated over all spectral components:

$$loss_{filter}(\tau_s) = 1 - \frac{\int a(\omega)|F(\omega)|\, d\omega}{\int a(\omega)\, d\omega} \tag{3.5}$$

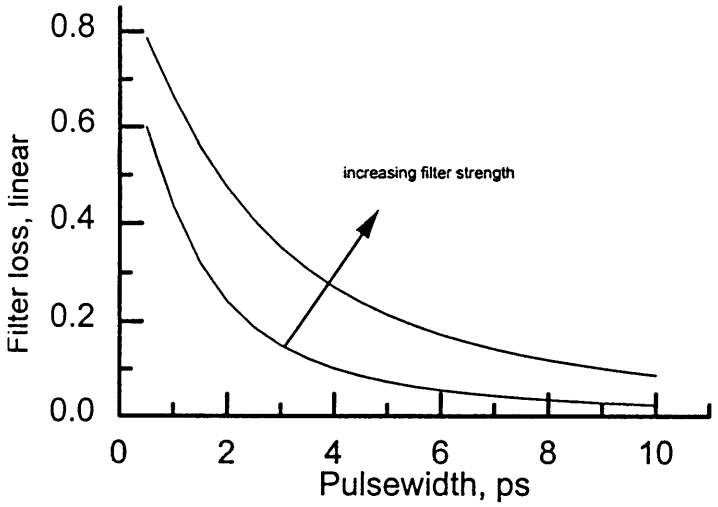

Figure 3-6: Filter loss for a 2^{nd} order bandpass filter as a function of pulsewidth. Both the absolute loss and rate of loss with small changes in τ_s increase with increasing filter strength, as expected. We have assumed that the pulse center frequency and filter center frequency coincide. The y-axis has been normalized such that a filter loss of 1 corresponds to zero transmission through the filter

For the soliton, we can write

$$a(t) = \sqrt{P_s}\, sech\left(\frac{t}{\tau_s}\right) e^{j\phi_{nl}}; \quad (3.6)$$

$$a(\omega) = sech\left(\frac{\pi}{2}\tau_s|\omega|\right) \quad (3.7)$$

where $a(\omega)$ is the Fourier transform, normalized by $\pi\tau_s\sqrt{P_s}$. A plot of the filter loss as a function of τ_s is given in figure 3-6.

We see that both the absolute loss and rate of loss increases with decreasing pulsewidth: $\Delta loss_{filter} \propto (1/\tau_s^2)\Delta\tau_s$. In the steady-state, low-intensity, wide pulses experience less loss at the filter, thus build up through repeated round trips through the erbium gain. The increasing intensity effectively leads to a shorter pulse through soliton effects until the pulse begins to experience loss at the filter. The steady-state loss for the train of pulses is least, then, for a completely-filled train of wider pulses than for a few, very short pulses with the same energy content.

Notice from table 3.1 that the supermode suppresion increased going from the 6.5

nm filter to the 20 nm filter even while the ratio of the pulse spectrum–compared to the filter spectrum–decreased, which indicates that the suppression mechanism is nonlinear. Dynamically, then, how the filter contributes to pulse-to-pulse stability is through the action of SPM: an instantaneous increase in photon number increases the peak power instantaneously. The pulse then accumulates an additional nonlinear phase shift with propagations as

$$\phi_{nl} = \delta(P_s + \Delta P_s)L \tag{3.8}$$

which appears as a frequency chirp ($\delta\omega = -\partial\phi(t)\partial t$) in the wings of the pulse. The equivalent change in photon number is more effective in generating spectrum for a more narrow pulse than a fatter one. The additional spectral components are removed by the filter. Because SPM accumulates with propagation, we would expect that the relevant distance is on the order of a soliton period. From the data of table 3.1, that works out to 50, 3, and 1 round trips for the 4.2 ps, 1.0 ps, and 600 fs pulses, respectively.

3.6 Modulator-induced Loss

An alternative explanation that could account for increasing loss for shorter pulses comes from the perturbation theory [21]. It shows that the perturbations relevant for the active modelocking case (without APM action) are those governing the pulse center frequency Δp and timing ΔT:

$$T_R \frac{\partial}{\partial T}\Delta p = -\frac{1}{\tau_s}\Delta p \tag{3.9}$$

$$T_R \frac{\partial}{\partial T}\Delta T = \delta T_0 + -\tau^2 \frac{\pi^2}{6} M\omega_m^2 \Delta T + 2|D|\Delta p \tag{3.10}$$

where δT_0 is the temporal detuning between the modulator and laser roundtrip time. In the steady state, we find that

$$\Delta p_{ss} = 0 \tag{3.11}$$

$$\Delta T_{ss} = -\frac{\delta T_0}{\tau^2 \frac{\pi^2}{6}} M\omega_m \tag{3.12}$$

Timing restoration falls off like the square of the pulsewidth. Thus, a short pulse will sit farther in the wings of the modulation function than a wide pulse. The absolute loss is given by

$$loss_{AM} = 1 - cos(\omega_m \Delta T_{ss}) \tag{3.13}$$

Of course, for any given pulsewidth, the strength of timing restoration must increase with ΔT, else the modulator would be unable to restore timing for any amount of detuning. The pulse would drift away from the modulation peak, move out into the wings of the transmission function, and modelocking would cease. The strength of the retiming strength is given as $\partial loss_{AM}/\partial \Delta T$, which does increases for larger ΔT. The importance of (3.12) is that it suggests that shorter pulses experience a weaker restoring force at a given ΔT than a longer pulse, and thus will move farther out into the modulator wings where the restoring force increases. And since the absolute loss increases with ΔT, shorter pulses see a larger absolute loss than larger pulses for a given frequency detuning. The relevant time scale compared to the case of SPM + filtering is also on the order of round trips.

3.7 Experimental Considerations

3.7.1 Modulator Bias

The amplitude modulator biasing curve, displayed in figure 3-7, was recorded by varying the dc voltage to the modulator with the rf voltage set to zero and monitoring the laser output power. The transmission curve for an amplitude modulator varies as $\cos^2(V_{bias})$ as shown in Chapter 1, but here the device is operating in a laser, thus increasing the loss of the modulator decreases the slope of the output laser power characteristic with varying pump power, displayed in figure 3-8. The curve of figure 3-7 can be extracted by moving down a vertical of figure 3-8. Note that increasing the linear loss eventually brings the laser below threshold where the output power is solely ASE.

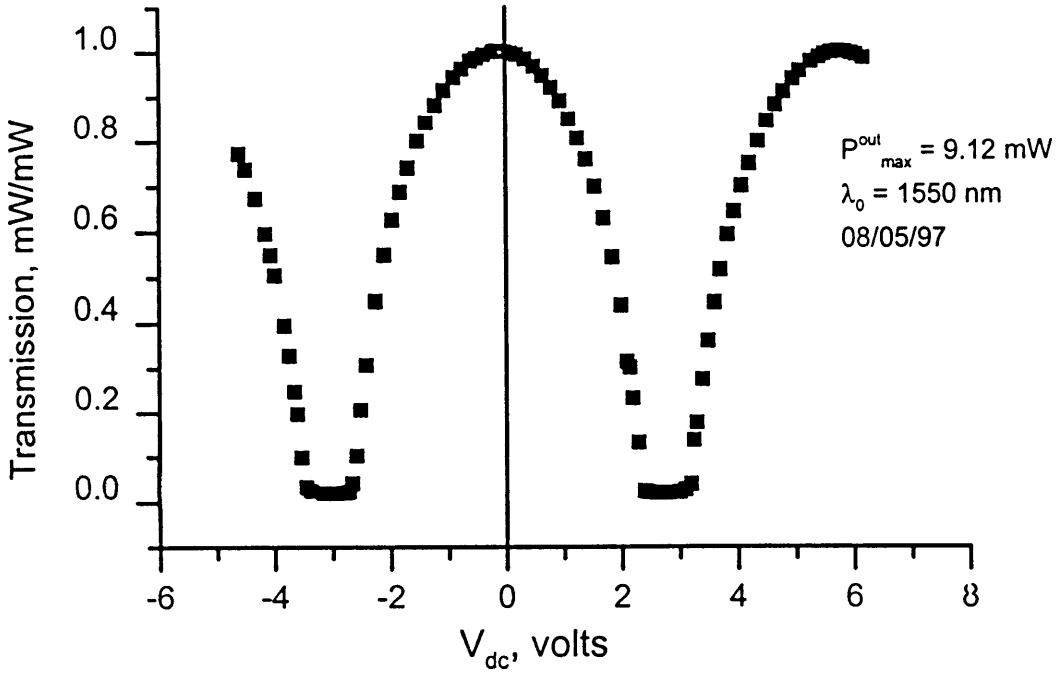

Figure 3-7: Laser output power versus modulator bias voltage. The rf applied voltage is zero, and the laser is running cw.

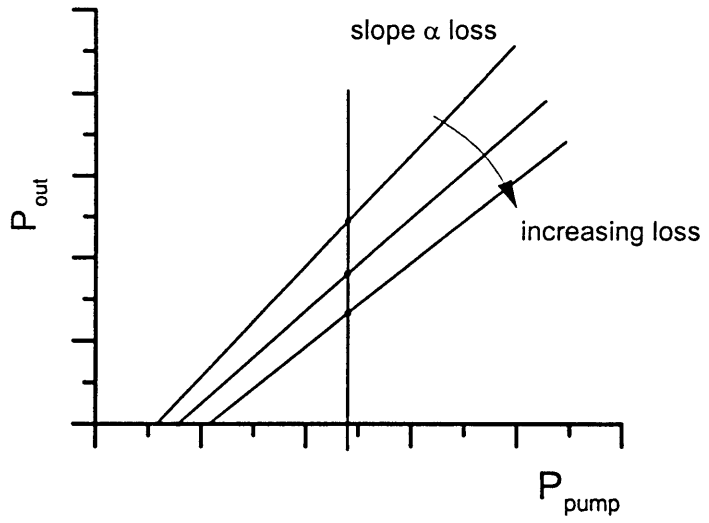

Figure 3-8: Example of output power variation with increasing linear loss as a function of pump power

3.7.2 Modulator Chirp

The modulator was operated in push-pull mode and biased at the 3-dB point where the modulator chirp is theoretically zero. Chirp in this context is defined as the ratio of phase modulation to amplitude modulation. Changing the amplitude of the relative voltage levels between pushing and pulling arms of the amplitude modulator and operating at various bias points does give one the freedom to adjust the modulator chirp between ± 1. While chirping may have some advantages [2], it was not pursued here–more details can be found in the appendix.

3.8 Conclusions from AML

So, what we have learned from the work in this chapter is the following:

- The shortest pulses and best pulse-to-pulse amplitude fluctuation suppression were achieved with the 20 nm filter. For 350 mW of 980 nm pump, we could obtain pulses less than 600 fs with better than -45 dB suppression of the supermodes. With ϕ_{nl} on the order of $2\pi/8$ for the 600 fs pulse, the pulse is close to sideband-limited. The modulator strength was not critical and could be varied by 2-3 dB without visibly affecting the pulse parameters.

- The suppression of the supermodes increased with the broadest bandwidth filters and the shortest pulses. We have suggested three mechanisms: sideband limiting, SPM + filtering, and modulator-induced loss. A more careful study of the stability mechanism at work will be investigated further.

- Without intervention, the laser remained stable for, at most, five to ten minutes without intervention. The laser could be maintained indefinitely with slight adjustments to both the modulator frequency and bias voltage.

Chapter 4

Regenerative Modelocking

As discussed in chapter one, the motivation for stabilizing an actively modelocked laser is to ensure that the detuning between the laser frequency at ω_c and the modulation frequency ω_m is less than approximately 10 kHz to maintain modelocking in the presence of the thermal drift and other environmental perturbations. Many groups have attempted stabilizing the laser cavity via piezo-electric control, while the external modulation function ω_m is kept constant–see the references mentioned in chapter one. Thus, the oscillation frequency ω_c remains constant. The regenerative approach allows ω_c to drift freely and fixes the modulation frequency to follow ω_c. In this chapter, we will experimentally explore the later technique.

4.1 Key differences between RML and AML

We will define a frequency detuning ω_d between $N\omega_c$ and ω_m, the repetition rate and modulator frequency, as

$$\omega_d = N\omega_c - \omega_m = \frac{\partial}{\partial T}\phi \tag{4.1}$$

where N is an integer, indicative of harmonic modelocking. For AML without stabilization, $\omega_d \neq 0 \leq \omega_d^{max}$, and no fixed phase relationship exists between the modelocker and the laser pulse. ω_d drives the evolution of the relative phase between them, and in time, the pulse walks off the modulation center, and ΔT increases as shown in figure 4-1. Notice that δT is greatly exaggerated here for clarity. The restoring force

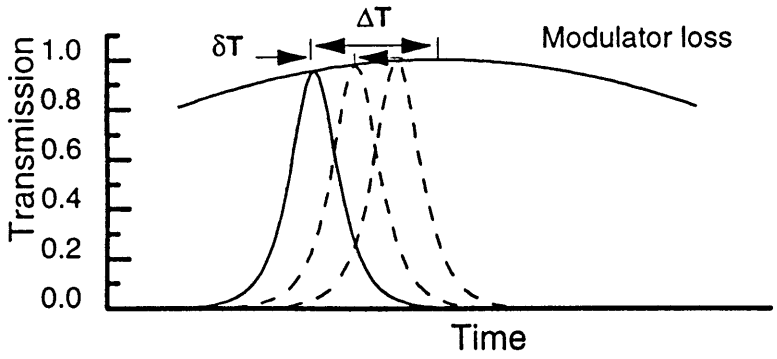

Figure 4-1: Relationship between the pulse and modulator transmission peak. Δ T is the offset of the pulse from the modulation peak (mimimum loss), and δ T is the amount of retiming the modulator imparts to the pulse per round trip.

imparted by the modelocker provides a push δT to the pulse that makes up for the roundtrip phase difference between the laser and modulator oscillation frequencies. The restoring force is zero for $\Delta T = 0$, and increases as $\mathrm{Msin}^2[\omega_m(\Delta T)]$.

For RML, the modulation frequency is derived from the oscillation frequency, so $\omega_d = 0$. The phase between the modulator and laser are not driven, and there will exist a fixed phase relationship between the two:

$$\begin{aligned} \omega_d &= \frac{d}{dT}\phi = 0; \\ \phi &= \phi_0(\omega) \end{aligned}$$

For reference, we will define $\phi = 0$ as zero offset between the peak of the modulation function and the arrival of the pulse so that $\Delta T = 0$, representing the difference in arrival times of the pulse train at the modulator and the electrical path delay. So, $\Delta T = \phi_0(\omega)$. We have explicitly shown the frequency dependence of ϕ_0, as will be explained in more detail in the following section. In response to cavity drift, $\omega_c \Longrightarrow \acute{\omega_c}$, thus $\acute{\omega_m} = \acute{\omega_c}$. The new pulse position will be $\Delta\acute{T}$. If the electrical delay time is not frequency dependent–true for the optical path–then the pulse will

sit under the modulation function with a fixed ΔT.

Notice from figure 4-2 that the phase difference is set manually in the clock extraction circuit. The setting of ϕ_0 is not critical and should be allowable to the limits described for detuning above.

The power delivered to the modelocker in AML is determined externally; for the RML, the power delivered is weakly dependent on the input signal power–here, we have ensured that the last stage of amplification is operating in deep saturation, followed by a variable attenuator. Thus, small amplitude fluctuations will not drive large swings in the power delivered to the modulator. One could imagine a situation in which the loop gain is set such that the oscillation condition is marginally stable with a strong restoring force, possibly leading to chaotic pulse patterning, but such a condition was not explored here.

For RML, characteristics of the startup properties can be likened to those of a passive modulator in that the clock extraction circuit preferentially amplifies noise spikes occurring in the range of 10 GHz and begins to drive the modulator, giving positive feedback in the initiation of modelocking. We should note here that, unlike a phase-locked loop, there is no integrating action in the clock extraction circuit that inhibits startup while also suppressing small changes in the input amplitude on the modulation signal. In effect, our clock extraction circuit is virtually memoryless.

4.2 Experimental Setup

The setup as shown in figure 4-2 is the same as that in figure 3-1, but with the clock extraction circuit replacing the external signal source driving the modulator.

4.3 Theory of Operation

In this section, we will make explicit the operation of the regenerative feedback action and derive the governing equations that determine the oscillation frequency and loop gain.

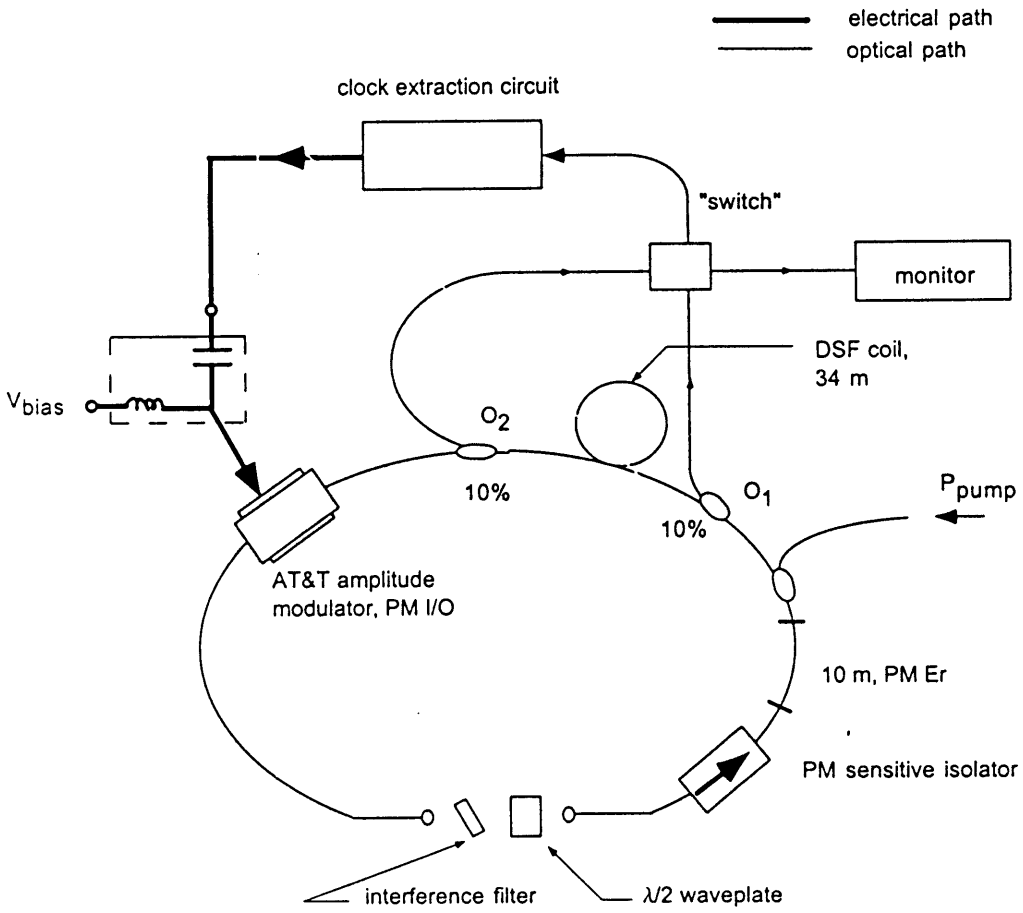

Figure 4-2: Experimental setup for RML

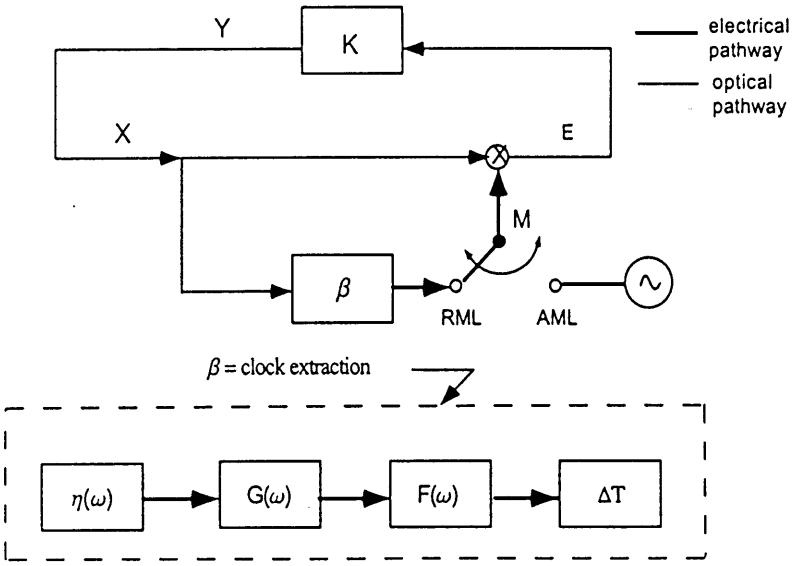

Figure 4-3: Regen model: a systems perspective

Consider the model shown in figure 4-3. $K(\omega)$ is the frequency response of the cavity operators for dispersion and SPM. $Y(\omega)$ is the optical signal following the modulator, denoted by $\otimes$, and $X(\omega)$ is the optical signal just before the output coupler to the clock extraction circuit. The transfer functions for each of the discrete devices in the clock extraction circuit $\beta(\omega)$ are $\eta(\omega)$ for the photodetector, $F(\omega)$ for the rf bandpass filter, ΔT for the action of the rf phase shifter, and $G(\omega)$ for the amplifier. The path from β to the modulator is electrical, while all other paths are optical. Notice that we have included a switch here to differentiate between the AML with no feedback and RML.

The equations of operation are given below: we will switch between time and frequency domain via Fourier transforms, denoting the transformation with either time or frequency as the function argument. The modulated signal Y(t) is given as

$$Y(t) = M(t)X(t)\,e^{j\phi_{L1}} \tag{4.2}$$

where ϕ_{L1} is the optical phase delay between the output coupler and modulator. For the AML case, M(t) is the signal generator output, as shown. In the frequency domain,

$$Y(\omega) = M(\omega) * X(\omega)e^{j\phi_{L1}} \tag{4.3}$$

where $*$ is the convolution operator. The feedback is given as

$$M(\omega) = \beta(\omega)X(\omega)e^{j\phi_e} \tag{4.4}$$

where ϕ_e is the accumulated phase shift of the electrical signal through the clock extraction circuit. Solving the above equations, we find that

$$Y(\omega) = [\beta(\omega)X(\omega)e^{j\phi_e}] * X(\omega)e^{j\phi_{L1}} \tag{4.5}$$

$$= [\beta(\omega)X(\omega)e^{j\phi_e}] * [K(\omega)Y(\omega)e^{j\phi_{h\nu}}] \tag{4.6}$$

where all of the feedback operators are contained in the $\beta(\omega)$ term, and $\phi_{h\nu}$ is the total optical phase delay accumulated around the cavity. From 4.6, we find that

$$\beta(\omega)K(\omega)X(\omega)e^{j(\phi_{h\nu}+\phi_e)} = 1 \tag{4.7}$$

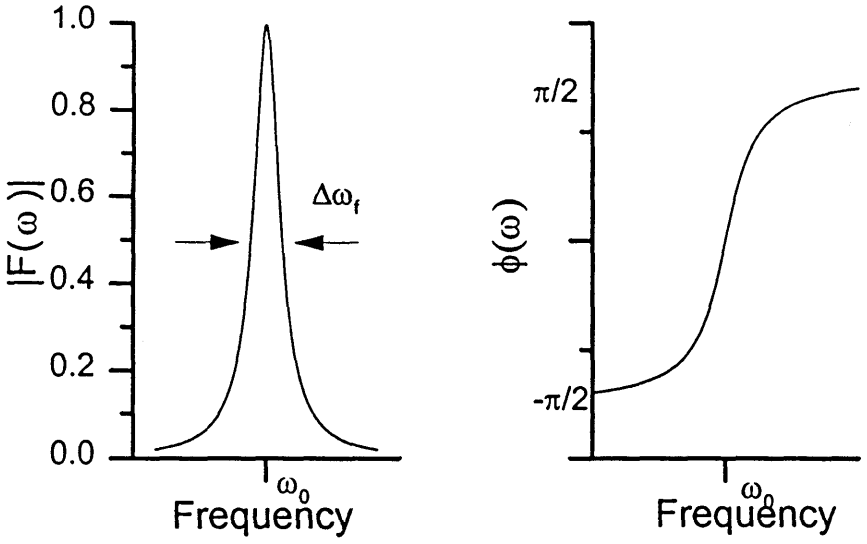

Figure 4-4: 2^{nd} Order filter, bandpass $\Delta\omega_f$; amplitude and phase response

For our wideband photodetector and amplifier, we can write $\eta(\omega) = \eta$, $G(\omega) = G$, and the frequency response of the laser can be written $K(\omega) = K$. Including the clock extraction operators in place of β, we find that

$$\eta G K X(\omega) F(\omega) e^{j(\phi_{h\nu}+\phi_e)} = 1 \tag{4.8}$$

The real parts of equation 4.8 define the loop gain, and the imaginary parts, the oscillation frequency. We will assume a simple filter of second order with 3dB bandpass $\Delta\omega$ and centered at ω_0, shown in figure 4-4. Notice that the more narrow the bandpass, the greater the phase slope.

$$\begin{aligned} F(\omega) &= \frac{\omega}{\omega + j\frac{\omega^2-\omega_0^2}{\Delta\omega_f}} \\ &= |F(\omega)|e^{-j\phi_{rffilter}} \end{aligned} \tag{4.9}$$

So, the imaginary parts yield

$$\phi_{h\nu}(\omega) + \phi_e(\omega) - \phi_{rffilter}(\omega) = 2m\pi \tag{4.10}$$

with m=0, 1, 2, etc..., and where

$$\phi_{rffilter} = \arctan\left[-\frac{1}{\omega}\frac{\omega^2-\omega_0^2}{\Delta\omega_f}\right] \tag{4.11}$$

Actually, we can relax the equal sign in 4.10 since the arrival time of the pulse coinciding with the peak of the modulation signal can be mismatched by the amount given by the maximum restoring force of the modulator, as discussed in a previous section. That is, $\phi_0 = \phi_{h\nu}(\omega) + \phi_e(\omega) - \phi_{rffilter}(\omega) - 2m\pi$. The real parts give the next equation

$$\eta GKX(\omega)|F(\omega)| = 1 \tag{4.12}$$

From (4.10) and (4.12), we can find 1) the oscillation frequency $N\omega_c$, which must lie within the pass band of the filter, around 10 GHz, and 2) the loop gain required to maintain steady-state oscillation at the steady-state osciallation frequency.

4.4 Experiments

From previous experiments with AML, we found that with approximately 350 mW of pump power at 980 nm, we could generate pulses as short as 600 fs with rf sideband suppression below -45 dB. With the results of the experiments presented in chapter three, we can benchmark the performance of RML with AML with respect to 1) pulse shaping, 2) suppression of pulse-to-pulse amplitude fluctuations, and 2)long-term stability. At the least, we need to show that RML will maintain long-term modelocking without degradation of the pulse train. Our plan below then is as follows:

- repeat the previous experiments for AML; namely, with the pump power held constant, monitor the effects of optical filter strength on the laser performance. We expect that the results will be the same as for AML.
- establish that the RML clock extraction circuit scheme is able to follow changes in ω_c
- address the relevant issues that limit the RML scheme in maintaining long-term stability

	AML		RML	
filter, nm	τ, ps	rf sidebands, dB	τ, ps	rf sidebands, dB
2.5	4.6	-30 ± 2	3.6	-48 ± 2
6.5	1.0	-40 ± 2	.980	-50 ± 2
20	.600	-45 ± 2	—	—

Table 4.1: AML and RML results for varying filter strength; τ is the fwhm value, and rf sidebands refer to the magnitude of the rf sidelobes spaced by the cavity axial mode frequency, thus at 10 GHz $\pm n3.667$ MHz, where n = 1,2,3,... until the next modelocked component around 20 GHz.

4.5 Results and Analysis

Table 4.1 displays the results of varying filter strength on RML laser performance compared with AML [1]. We did not expect to see any significant differences in pulse-shaping between AML and RML, and the data given in the table supports that.

Figure 4-5 shows a representative spectra for the regenerative and active cases for the 6.5 nm filter, and an autocorrelation trace of the RML .980 ps pulse is shown in figure 4-6. We did notice a slight asymmetry in the RML spectra compared with AML for all optical filter strengths, consistent with that observed by another group [34]. At present, we do not have a good explanation for this observed asymmetry.

From figure 4-5 and the data given in the table, the sidemode suppression is enhanced by 10-15 dB.

This dramatic increase in noise reduction was rather unexpected. We had expected that while the RML would be able to withstand large environmental perturbations, thus maintaining the modelocked state on a long time scale, it should not be any more effective in noise cleanup on the time scale of round trips than AML. Notice that for AML, the next harmonic is 3.667 MHz away, clearly much farther than that allowed by the detuning limit of approximately 100 kHz. So, the AML is not allowed to switch from the Nth harmonic to the N $\pm 1^{th}$ harmonic, and each pulse will undergo its own

[1] data for the 20 nm filter was not available at the time of this write-up

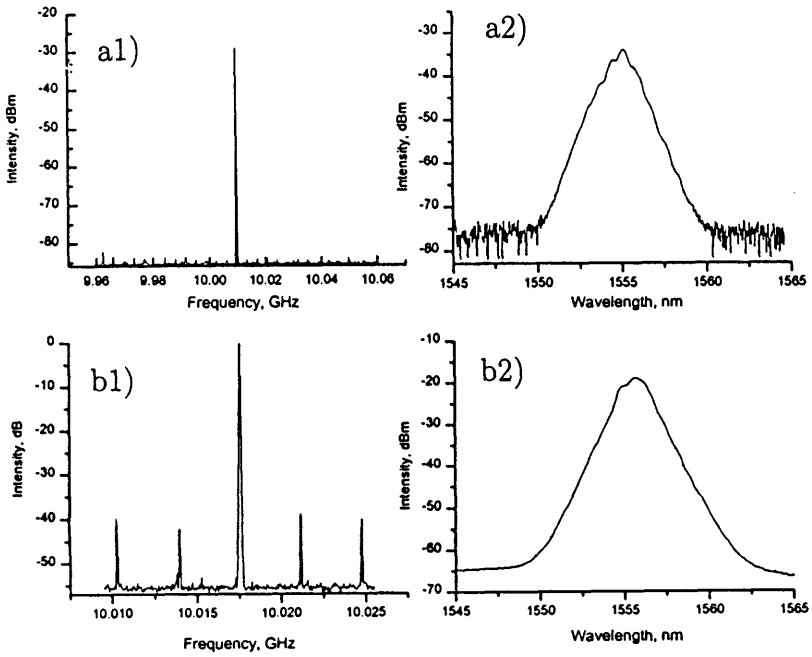

Figure 4-5: Lasing characteristics of RML and AML at 10 GHz; 6.5 nm filter. a1)RML rf spectrum, a2) RML optical spectrum, b1) AML rf spectrum, b2) AML optical spectrum. Notice that the scales for the two rf spectra are different

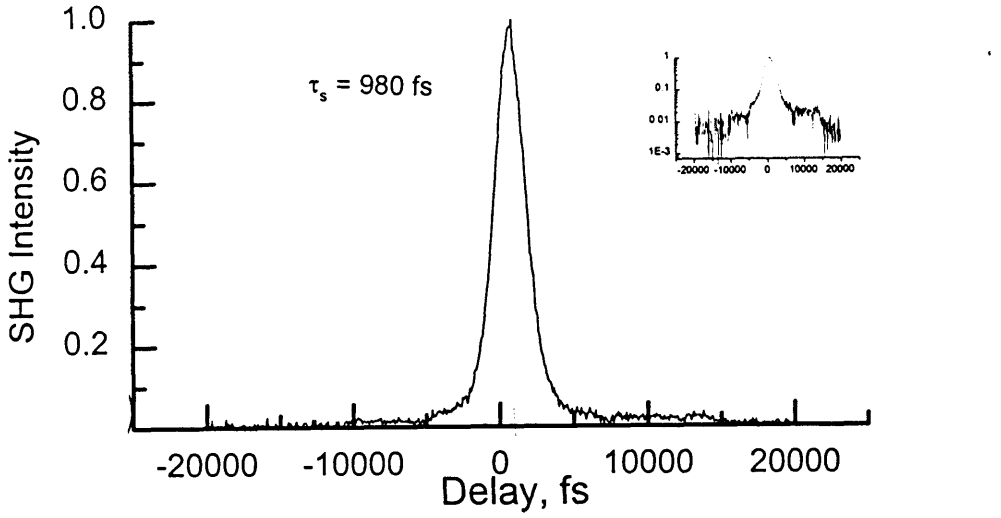

Figure 4-6: Autocorrelation of the RML for a 6.5 nm filter; inset shows the continuum suppressed by 20 dB in the wings of the pulse on a semilog plot

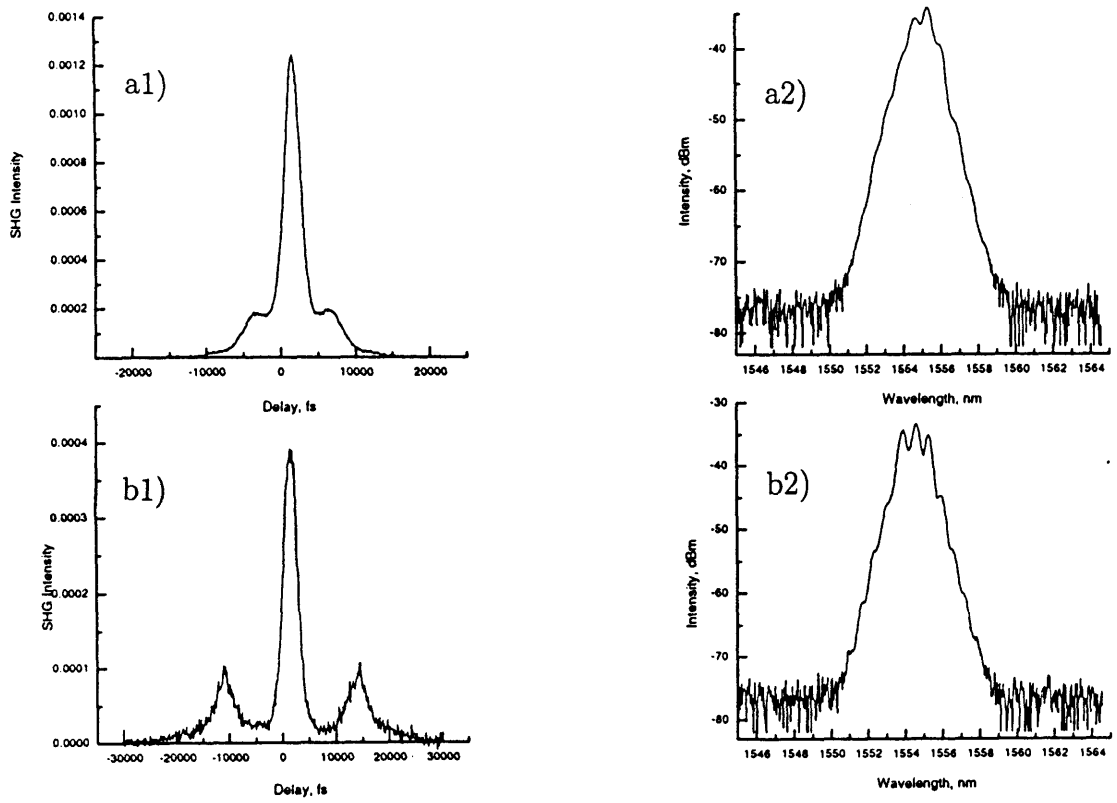

Figure 4-7: Autocorrelations of RML with a 6.5 nm filter. a1) autocorrelation with apparent satellite pulse (ratio of 1:6) separated from the main pulse by 5 ps; a2) its corresponding optical spectrum, fringe spacings on the order of .6 nm; b1) autocorrelation of same system with satellite pulse (ratio of 1:4) separated by 15 ps; b2) corresponding optical spectrum, fringe spacings of .65 nm

dynamics in its time slot. In contrast, for RML, we could switch from supermode to supermode simply by changing the electrical phase delay.

Related to the above is the occasional observation of satellite pulses for RML shown in figure 4-7. The 4:1 and 6:1 amplitude ratios between the main peak and the satellite indicates that the satellite amplitude is less than 50 % of the main pulse. We did not observe any instances of satellite pulses for AML.

One possible explanation for the formation of the satellite pulse is as follows: consider a large phase setting ϕ_0 between the modulator envelope and laser oscillation frequency such that the pulse sits far from the modulation peak. Another pulse could build up in the same time slot just behind the first. The first pulse suffers more and more loss and slides further out into the wings of the modulator transmission, leaving

more gain for the second pulse. Because of the fixed ϕ_0 setting, the second pulse will then slide out into the wings of the modulator transmission. Another pulse starts to build up near the modulation peak, thus the continual birth/death cycle of pulses–the absolute phase just accumulates linearly. For case b), the .65 nm fringes corresponds to an equivalent 1.3 mm Fabry-Perot cavity, indicating a possible reflection from the interference filter or other within the cavity as the seeding pulse. However, that fringes are also evident in the AML case shown in figure a) suggests that another mechanism could be at work in RML supporting the formation of satellite pulses.

In each of the measurements, we could track the change in the oscillation frequency on the rf spectrum analyzer. We observed that the laser oscillation frequency varied by $\pm$ 5 to 10 kHz. The noise structure around the 10 GHz oscillation did not change as the frequency drifted, which is a good indication that the clock extraction circuit was tracking the modulation frequency ω_m to the changing cavity frequency ω_c on a time scale much faster than the relaxation oscillations that occur typically around $\pm$100 kHz. In contrast, for AML one observes a growth in the relaxation oscillations as thermal cavity expansions begin pulling ω_c away from ω_m.

Without intervention, the laser was observed to run for 15-20 minutes without noticeable changes in the optical or rf spectrum, or on the pulsewidth. Small readjustments to both the phase delay and dc bias to the modulator were necessary to maintain the single supermode state for longer times. While the exact cause for the instability has not been determined, evidence suggests that drift of the modulator bias may be the main cause. The bias curve as shown in figure 3-7 was seen to drift by as much as one volt within 24 hours (but the total voltage swing needed to turn the device on/off did not change, of course). For reference, the total voltage swing needed to turn the device on/off is only 3 volts. However, since we did need to slightly adjust the rf phase, another contribution could be that the frequency-dependence of the rf phase contributes to a shifting of the relative phase between the modulator and laser pulse train. For our second order filter, we find that

$$\frac{d}{d\omega}\phi_{rffilter} = \frac{1}{1+\left(\frac{\omega^2-\omega_0^2}{\omega\Delta\omega_f}\right)^2}\frac{\omega^2+\omega_0^2}{\omega^2\Delta\omega_f} \tag{4.13}$$

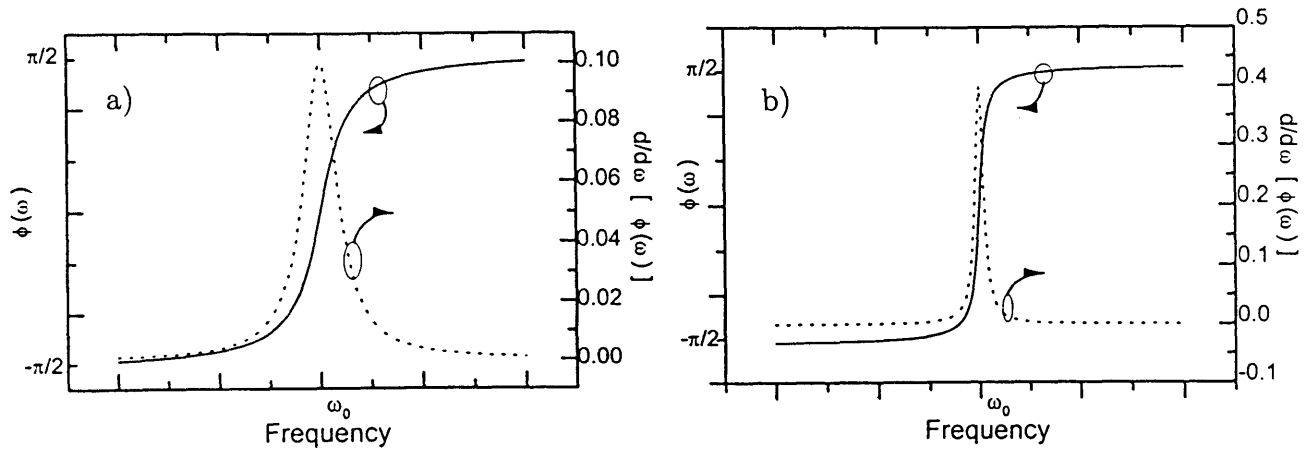

Figure 4-8: Phase-slope superimposed on frequency-response plot for the phase of a bandpass filter with 3-db bandwidths of a) 20 MHz and b) 5 MHz filter. Notice that the scales for the two filter bandwidths are not the same.

In figure 4-8, we show the magnitude of the derivative for both a 5 MHz and 20 MHz filter centered at 10 GHz. The filter used in our experiment is a 6th order Chebyshev filter and will experience a much larger derivative than that shown for the 2_{nd} order filter here. In the figure, we see that decreasing the bandwidth by factor of four increases the phase slope by a factor of two.

4.6 Conclusions from RML

- For equivalent modulation strength and optical filter strength, the RML scheme exhibits pulses almost identical to those of AML. However, the pulse spectra for RML are slightly asymmetric compared to AML, and satellite pulses were occasionally observed for RML. We made a plausiblity argument for the orgin of the satellite pulses based on the difference between the arrival times of the electrical and optical signals to the modulator set by the phase bias in the clock extraction circuit.

- For the same pulse parameters (i.e, pulse energy, spectrum, pulse width), the RML scheme is much more effective than AML without stabilization in suppressing amplitude fluctuations. From the previous chapter, we suggested three possible mechanism enforcing pulse-to-pulse stability. While the action of both sideband limiting and SPM + filtering would be similar for both AML and RML, the case for modulator-induced loss should be quite different for RML compared to AML and deserves further investigation.

- The RML laser remained stable for 15-20 minutes without intervention. The limiting factors for stability are most likely the drifting modulator bias voltage and probably less so on the frequency-dependent phase difference in the clock extraction circuit. The exact cause will be determined in future work.

Chapter 5

Summary and Future Work

The motivation for this work was to build a stable, 10 GHz source of picosecond pulses. We can report here that we have constructed a source that produces sub-picosecond pulses at 10 GHz with rf suppression on the order of 55 to 60 dB, and the long-term stability of the laser seems to be limited by the drifting bias of the amplitude modulator.

We have presented the governing equations for regenerative feedback and compared its performance with that of an unstabilized cavity. We found that RML exhibited similar pulse shaping , as we expecte, but RML also increased the rf stability by at least 10 to 15 dB. We found that relaxing the filter strength such that the pulse spectrum is much smaller than the filtering strength led to both shorter pulses as well as a reduction in pulse-to-pulse amplitude fluctuations. We presented plausibility arguments for three mechanisms that can explain a pulsewidth-dependent loss (spectral limiting)–soliton sideband limiting, SPM + filtering, and modulator-induced loss. While much progress has been reported in this thesis, much work must be done before it can be used as a reliabe source for real a system, including the following:

- Stabilize the bias voltage via feedback circuitry–we saw that the laser was not able to stay modelocked for more than 30 minutes without one needing to tweek the bias voltage and, occasionally, the rf phase delay, to maintain stable

operation. Too, we will try RML with phase modulation–if successful, we will be able to eliminating the bias-drift problem altogether since no bias is required.

- Test the stability of the system as a function of pump power. The data here, given for a fixed pump power, does not illuminate the stabilization mechanism at work. While we have made plausibility arguments for three mechanisms that impart a pulsewidth-dependent (spectrum dependent)loss explaining how relaxing the filter strength leads to increased pulse-to-pulse stability in which the filter bandwidth $\gg$ spectral bandwidth, a more complete stability analysis in the spirit of Namiki et al [36] is required in which the rf spectrum, optical spectrum, and output power are monitored as a function of increasing/decreasing the pumping rate.

- Test the effects of a longer/shorter section of DSF fiber. The length of the DSF spool we included in our laser was for dispersion management and to increase the nonlinearity by a factor scaled to a system that has worked regeneratively (i.e., our power is three to four times larger, and the spool of DSF is 4-5 times shorter).

- Verify the importance of the phase-slope dictated by a narrow bandpass filter. The phase slope was given here for a second order filter, but we have not conclusively determined the importance of that magnitude–it may be that when setting the phase initially, the pulse finds a position where the phase-slope is least.

- The laser only self-started a fraction of the time–this may be related to the issue of phase control and where the system is most stable upon startup.

- Demonstrate that the laser can be tuned while modelocked, and compare the performance of RML across the erbium bandwidth.

- It should be an interesting task to consider the stabilization strength of saturated APM with the above stabilization schemes of SPM + filter and modulator

effects. In the case of APM, one can achieve limiting action of APL by over driving the self-amplitude coefficient, modeled as $\gamma_3|a|^2 - \gamma_5|a|^4$. APM/APL is interferometric in nature, thus the effect saturates beyond a given intensity. It may also be that the built-up energy in the continuum, particularly for a high-Q cavity, couples back to the soliton, thus providing a means for the photons from extremely short pulses (photon rich) to transfer energy to the wider (photon poor pulses), but that coupling would be at most of second order in the coupling coefficient.

Appendix A

Clock Extraction Hardware

In the following sections, the electronics employed for clock extraction will be described.

A.0.1 Photodetector

141x New Focus, InGaAs, rise time of 17 ps; max conv. gain = 15 V/W, yielding -39.2 dBm output for a 1 mW cw input. The response is nearly flat out to 60 GHz, then the responsivity drops sharply due to the RC pole from the diode in addition to other parasitic poles [37].

A.0.2 Amplifiers

Figures A-1 through A-3 depict the amplifiers' performance. While the minimum requirement of the amplifier is to achieve unity loop gain, as discussed in chapter four, we would like the clock extraction circuit to have a very weak dependence on input power so that small amplitude fluctuations at the input to the photodetector around P_{in} do not translate into large fluctuations at the output once P_{in} is greater than some saturation power. Achieving saturated performance at the last stage of amplification requires that the output power of the first power amplifier be enough to push the last amplifier into saturation. From Figure A-3, the last-stage power amp exhibits a 1-dB compression point of 30 dBm, requiring an input power of $P_3 > -10dBm$ (40

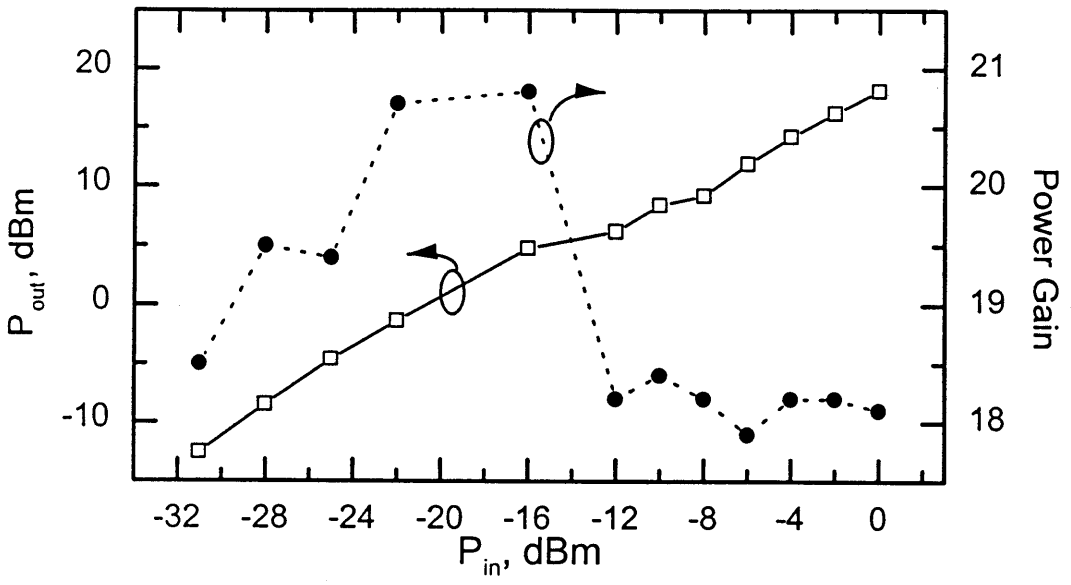

Figure A-1: 1422 New Focus preamplifier

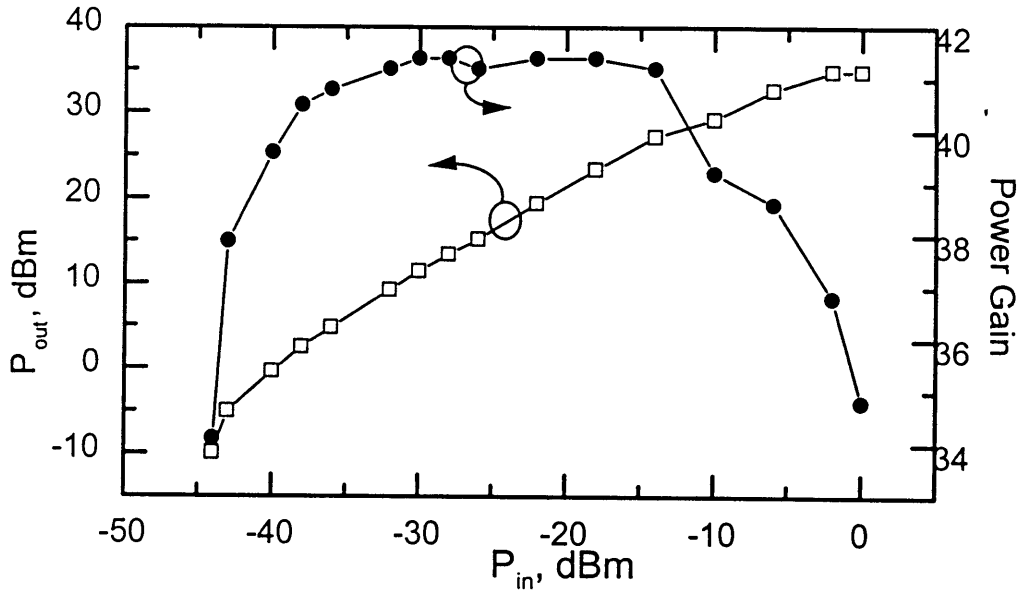

Figure A-2: APT18660 Avantek power amplifier

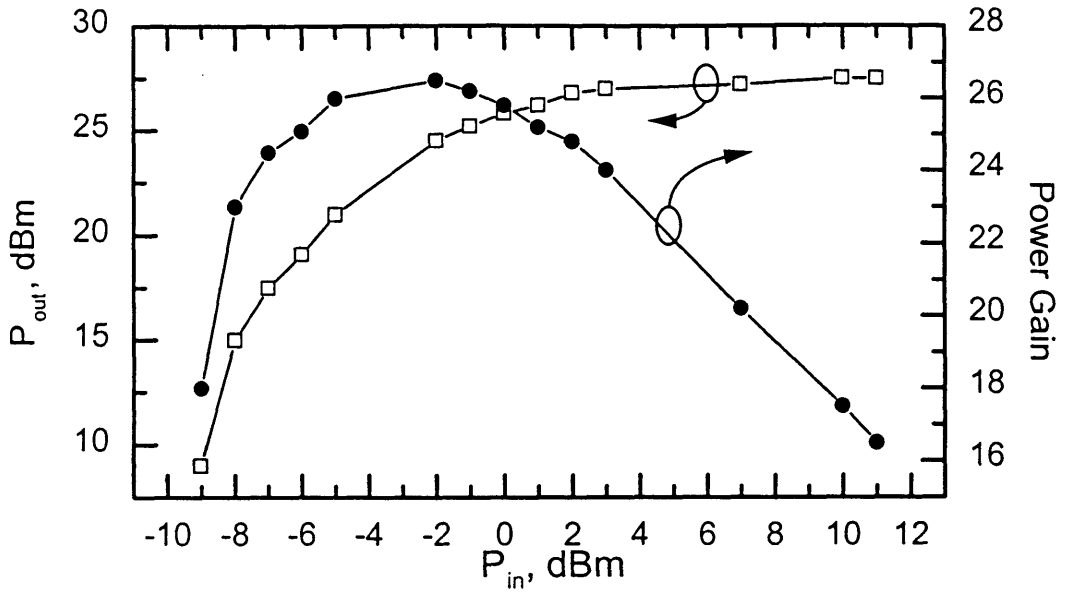

Figure A-3: APT3038 Avantek power amplifier

dB gain). Working backwards, we find that we can saturate the last amplifier with an input power > 55 dBm, requiring an input power (assuming nominal conversion efficiency) > 200μW, a condition easily met for our laser system.

A.0.3 rf Filter

The rf dielectric filter used here is a 6th order bandpass Chebyshev filter with a 3 dB bandwidth of 20 MHz, centered at the desired 10 GHz repetition rate (giving an effective filter Q of 500). For our cavity with a 3.667 MHz fundamental repetition rate, on the order of 20/3.7 = 6 to 7 supermodes exist that can potentially compete for gain.

A.0.4 rf Phase Shifter

The rf phase shifter is manually set by the adjustment of a plunger, making incremental adjustments difficult (approx 2 π radians/cm @ 10 GHz). The adjustment can be done with the clock extraction circuit operating in real time.

A.0.5 rf Attenuator

The attenuator can be varied in increments of 1 dB from 0 to 9 dB. While the attenuator can be switched with the clock extraction on, the attenuation between states does not vary smoothly. From the observed drop in power, the intermediate state resembles an open circuit. The variation from state-to-state entails a few milliseconds of delay.

Appendix B

Modulator-Induced Chirp

The following section describes the chirp imposed by an integrated amplitude modulator.

Considering the picture of the modulator, we will define a chirping factor that scales the amount of phase modulation resulting from amplitude modulation [2]:

$$\alpha = \frac{\left(\frac{d\phi}{dt}\right)}{\left(\frac{dS}{dt}\right)} \tag{B.1}$$

where ϕ is the average phase change in each arm $(\phi_2 + \phi_1)/2$, and S is the scaled intensity of the electric field at the output of the modulator

$$S = |E|^2 = S_0 \cos\left[\frac{\phi_2 - \phi_1}{2}\right] \tag{B.2}$$

For a dual-drive, we assume two sinusoidal driving voltages where

$$V_1(t) = V_1 \sin(\omega t) \tag{B.3}$$

$$V_2(t) = V_2 \sin(\omega t) + V_{bias} \tag{B.4}$$

We can relate how a change in voltage changes the index of refraction via the electrooptic effect [From Shen, Principles of Nonlinear Optics, 1984]:

$$\Delta n_k(t) = \Gamma_k \left(\frac{n_0^3}{2}\right) r_{xx} \left(\frac{V_k(t)}{d}\right) \tag{B.5}$$

$$= \eta_k V_k(t) \tag{B.6}$$

where Γ_k and r_{xx} are the overlap integral between electrical and optical fields and electrooptic tensor coefficient for the kth index along the xx direction. And the phase change in each arm of the interferometer is related to the index of refraction as

$$\phi_i = \frac{2\pi}{\lambda} n_i L \tag{B.7}$$

where L is the interaction length of the applied voltage with the optical field in each arm of the interferometer. So, we find the following expression for chirp:

$$\begin{aligned} \alpha &= \left(\frac{\eta_1 V_1 + \eta_2 V_2}{\eta_1 V_1 - \eta_2 V_2} \right) \\ &\quad \cdot \cot \left[\frac{\pi L}{\lambda v_{ac}} (\eta_2 V_2 \sin(\omega t) + \eta_2 V_{bias} - \eta_1 V_1 sin(\omega t)) \right] \end{aligned} \tag{B.8}$$

With the bias voltage set at the half-transmission point, $S = S_0/2$, and assuming that the same change in voltage induces the same change in the index of refraction in each arm of the interferometer, $\eta_1 = \eta_2$, and we find that

$$\alpha = \frac{V_1 + V_2}{V_1 - V_2} \tag{B.9}$$

and operating the modulator push-pull so that $V_1 = -V_2$, the chirp goes to zero. Driven single sided so that either V_1 or $V_2 = 0$, then the chirp is ± 1, and intermediate values can be accessed by modifying the relative amount of voltage on each arm.

Appendix C

Dispersion Measurements

Thanks to Dr. Brett Bouma for helpful discussions on the issue of dispersion and its measurement in lasers.

Methods for measuring intracavity dispersion vary, among them white light interferometry employing a cross-correlation of the ASE emerging from the cavity [?] and a frequency-domain technique in which the round-trip time of the laser is varied by tuning the lasing wavelength [29]. We employed the frequency-domain method here with one difference, as explained below.

Recalling that the second-order dispersion is given by

$$\beta'' = \frac{d}{d\omega}\beta' = \frac{d}{d\omega}\left(\frac{1}{v_g}\right) \tag{C.1}$$

where v_g is the group velocity dispersion; here, the units of dispersion are in ps^2/km. Or, in the venacular of wavelengths,

$$D = \frac{d}{d\lambda}\beta' = \frac{d}{d\lambda}\left(\frac{1}{v_g}\right) \tag{C.2}$$

where D is expressed in ps/nm/km. The technique employed by Knox et al [29] requires a means of tuning the laser while observing the repetition rate. For a passively modelocked source, observing the group delay as a function of wavelength can be measured down to Hz resolution with frequency counters. For an actively modelocked laser, one might expect that the rf phase noise would significantly degrade the resolution or that the resolution would be limited to within the detuning range of the

modelocker and the cavity length harmonic–typically on the order of kHz. We can remain in the frequency domain with our measurements by measuring the change in the repetition rate of a high harmonic as the laser is wavelength tuned while operating cw:

$$D = \frac{N}{L}\frac{d}{d\lambda}\left(\frac{1}{\nu_N}\right) \tag{C.3}$$

$$= \frac{n}{2\pi c}\frac{d}{d\lambda}\left(\frac{1}{\Delta\nu}\right) \tag{C.4}$$

where N is a harmonic of the cold cavity, thus $\nu_N = N \cdot \nu$. As long as one's system exhibits only a small contribution from nonlinear dispersion–as is the case for silica fiber–finding the dispersion while lasing cw rather than pulsed can at times be more convenient. The outstanding question then becomes one of resolution. The resolution of this dispersion measurement in finding the smallest change in ν_N must be the fwhm of the rf linewidth; so, we find that

$$D_{min} = \frac{N}{L}\frac{\delta\nu_N}{\nu_N^2}\frac{1}{\Delta\lambda} \tag{C.5}$$

$$= \frac{n}{2\pi c}\frac{\delta\nu_N}{\nu_N}\frac{1}{\Delta\lambda} \tag{C.6}$$

where $\Delta\lambda$ is the maximum tuning range of the laser. For $\Delta\lambda = 30$ nm, $\nu_N = 2\pi\times$ 1 GHz, and $\delta\nu_N$ expressed in kHz,

$$D_{min} = \frac{1.45}{36\pi^2}\delta\nu_N \tag{C.7}$$

yielding dispersion measurements good to within ± 0.204 ps/nm/km for a 50 kHz rf linewidth. The dispersion resolution is enhanced by

- tuning across the largest possible range, $\Delta\lambda$
- following the highest harmonic, ν_N

Bibliography

[1] K. A. Ahmed, H. F. Liu, N. Onodera, P. Lee, R. S. Tucker, and Y. Ogawa. Nearly transform-limited pulse (3.6 ps) generation from gain-switched 1.55 μm distributed feedback laser by using fiber compression technique. *Electron. Lett.*, 29:54–56, 1993.

[2] AT & T. *The Relationship between Chrip and Voltage for the AT & T Mach-Zender Lithium Noibate Modulators.*

[3] S. Bouchoiule, N. Stelmakh, M. Cavelier, and J.M. Lourtioz. Highly attenuating external cavity for picosecond-tunable pulse generation from gain/q-switched laser diodes. *IEEE J. Quantum Electron.*, 29:1693–1700, 1993.

[4] Anne-Marie Briancon, Bernard Jacquier, Jean-Claude Gacon, and Christian Le Sergent an Jean-Francois Marcerou. Inhomogeneous line broadening of optical transitions in Nd^{3+} and Er^{3+} doped preforms and fibers. *Fiber Laser Sources and Amplifiers II*, 1373:9–20, 1990.

[5] M. Cavelier, N. Stelmakh, J. M. Xie, L. Chusseau, J. M. Lourtioz, C. Kaxmierski, and N. Bouadma. Picosecond (2.5 ps) wavelength-tunable (20 nm) semiconductor laser pulses with repetition rates up to 12 GHz. *Electron. Lett.*, 28:224–226, 1992.

[6] S.V. Chernikov, M. J. Guy, J. R. Taylor, D.G. Moodie, and R. Kashap. Duration-tunable 0.2-20 ps 10 GHz source of transform-limited optical pulses based on an electroabsorption modulator. *Optics Letters*, 20:2399, 1995.

[7] D. Cotter. Technique for highly stable active mode-locking. In D.A. Auston and K.B. Eisenthal, editors, *Ultrafast Phenomena IV*, pages 78–80. Springer-Verlag, 1984.

[8] J. Debeau, L.P. Barry, and R. Boittin. Wavelength tunable pulse generation at 10 GHz by strong filtered feedack using a gain-switched fabry-perot laser. *Electron. Lett.*, 30:74–75, 1994.

[9] M. Dennis and I. N. Duling III. Experimental study of sideband generation in femtosecond fiber lasers. *IEEE Journal of Quantum Electronics*, 30:1469–1477, 1994.

[10] E. Desurvire. *Erbium-Doped Fiber Amplifiers: Principles and Applications.* John Wiley & Sons, Inc., 1994.

[11] J.N. Elgin and S.M.J. Kelly. Spectral modulation and the growth of resonant modes associated with periodically ampified solitons. *Optics Letters*, 18:787–789, 1993.

[12] J.P. Gordon. Dispersive perturbations of solitons of the the nonlinear schroedinger equation. *J. Opt. Soc. Am. B*, 9:91–97, 1992.

[13] S. Gray, A.B. Grudinin, W.H. Loh, and D. N. Payne. Femptosecond harmonically mode-locked fiber laser with time jitter below 1 ps. *Optics Letters*, 20:189–191, 1995.

[14] E.J. Greer, Y. Kimura, K. Suzuki, E. Yoshida, and M. Nakazawa. Generation of 1.2 ps, 10 GHz pulse train from all-optically modelocked, erbium fibre ring laser with active nonlinear polarization rotation. *Electronics Letters*, 30:1764–1765, 1994.

[15] P.J. Hardman, Paul D. Townsend, Alistair J. Poustie, and K.J. Blow. Expermental investigation of resonant enhancement of the acoustic interaction of optical pulses in an optical fiber. *Optics Letters*, 21:393, 1996.

[16] G.T. Harvey and L.F. Mollenauer. Harmonically mode-locked fiber ring laser with an internal fabry-perot stabilizer for soliton transmission. *Optics Letters*, 18:107–109, 1993.

[17] A. Hasegawa and F. Tappert. Transmission of stationary nonlinear optical pulses in dispersive dielectric fibers. I. Anomalous dispersion. *Appl. Phys. Lett.*, 23:142–144, 1973.

[18] A. Hasegawa and Kodoma Y. Signal transmission by optical solitons in monomode fibers. *Proc. IEEE*, 69:1145–1150, 1981.

[19] H.A. Haus. A theory of forced mode locking. *IEEE Journal of Quantum Electronics*, QE-11:323–330, 1975.

[20] H.A. Haus. *Waves and Fields in Optoelectronics.* Prentice Hall Series in Solid State Physical Electronics. Prentice Hall, 1984.

[21] H.A. Haus and A. Mecozzi. Long-term storage of a bit stream of solitons. *Optics Letters*, 17:1500–1502, 1992.

[22] H.A. Haus and Y. Silberberg. Laser mode locking with addition of nonlinear index. *IEEE Journal of Quantum Electronics*, QE-22:325–331, 1986.

[23] G.R. Huggett. Mode-locking of CW lasers by regenerative rf feedback. *Electronics Letters*, 30:186–187, 1994.

[24] E. P. Ippen, private communication, November 1995.

[25] E.P. Ippen. Principles of passive mode locking. *Appl. Phys. B*, 58:159–170, 1994.

[26] F.X. Kartner, D. Kopf, and U. Keller. Solitary-pulse stabilization and shortening in actively mode-locked lasers. *J. Opt. Soc. Am. B*, 12:486–496, 1995.

[27] S.M.J. Kelly. Characteristic sideband instability of peridocally amplified soliton. *Electronics Letters*, 28:806–807, 1992.

[28] T.S. Kinsel. A stabilized mode-locking Nd:YAlG laser using electronic feedback. *IEEE J. of Quantum Electron.*, QE-9:3–8, 1973.

[29] W. H. Knox. In situ measurement of complete intracavity dispersion in an operating ti:sapphire laser. *Optics Letters*, 17:514–516, 1992.

[30] S.K. Korotky and J.J. Veselka. In *Conference on Lasers and Electro-Optics*, OSA Technical Digest Series, page paper CPD25, Washington, D.C., 1993. Optical Society of America.

[31] Y. C. Lee and C. Shu. Optimized operation of self-seeded gain-switched lasder diode for electrically wavelength-tunable singlemode pulses. *IEEE Photon. Technol. Lett.*, 7:275–277, 1995.

[32] P.V. Mamyshev. Dual-wavelength source of high-repetition-rate, transform-limited optical pulses for soliton transmission. *Optics Letters*, 19:2074, 1994.

[33] Y. Matsui, H. Murai, S. Arahira, S. Kutsuzawa, and Y. Ogawa. 30-GHz bandwith 1.55μm strain-compensated InGaAs-InGaAsP MQE laser. *IEEE Photon. Technol. Lett.*, 9:25–27, 1997.

[34] M. Nakazawa, K. Tamura, and E. Yoshida. Supermode noise suppression in a harmonically modelocked fibre laser by self phase modulation and spectral filtering. *Electronics Letters*, 32:461, 1996.

[35] M. Nakazawa, E. Yoshida, and Y. Kimura. Ultrastable harmonically and regeneratively modelocked polarisation-maintaining erbium fibre ring laser. *Electonics Letters*, 30:1603–1605, 1994.

[36] S. Namiki, E. P. Ipppen, H. A. Haus, and C. X. Yu. Energy rate equations for modelocked lasers. *J. Opt. Soc. Am. B*, 14:1–13, 1997.

[37] New Focus. *Application Note 1: Insights into High-Speed Detectors and High-Frequency Techniques.*

[38] D.U. Noske, N. Pandit, and J.R. Taylor. Source of spectral and temporal instability in soliton fiber lasers. *Optics Letters*, 17:1515–1517, 1992.

[39] Th. Peiffer and G. Veith. 40 GHz pulse generation using a widely tunable all-polarization preserving erbium fibre ring laser. *Electronics Letters*, 28:1849–1850, 1993.

[40] D. S. Seo, H. F. Liu, D. Y. Kim, and D. D. Sampson. Injection power and wavelength dependence of an external-seeded gain-switched fabry-perot laser. *Appl. Phys. Lett.*, 67:1503–1505, 1995.

[41] X. Shan, D. Cleland, and A. Ellis. Stabilising with Er fibre soliton laser with pulse phase locking. *Electronics Letters*, 28:182–184, 1992.

[42] X. Shan and D.M. Spirit. Novel method to suppress noise in harmonically modelocked erbium fibre lasers. *Electronics Letters*, 29:979–981, 1993.

[43] A. E. Siegman. *Lasers*. University Science Books, 1986.

[44] M. Suzuki, H. Tanaka, N. Edagawa, K. Utaka, and Y. Matsushima. Transform-limited optical pulse generation up to 20 GHz repetition rate by a sinusoidally driven InGaAsP electroabsorption modulator. *J. Lightwave Technol.*, 11:468, 1993.

[45] E. A. Swanson, R.A. Barry, D. M. Castagnozzi, V.W.S. Chan, K.L. Hall, et al. All-Optical Network Consortium. Technical report, AT & T Bell Laboratories, Digital Equipment, Lincoln Laboratories, and Massachusetts Institute of Technology, 1995. ARPA-sponsored consortium.

[46] A. Takada and H. Miyazawa. 30 GHz picosecond pulse generation from actively mode-locked erbium-doped fibre laser. *Electronics Letters*, 26:216–217, 1990.

[47] H. Takara, S. Kawanishi, M. Saruwatari, and K. Noguchi. Generation of highly stable 20 GHz transform-limited optical pulses from actively mode-locked er-doped fibre lasers with an all polarization-maintaining ring cavity. *Electronics Letters*, 28:2095–2096, 1992.

[48] J.S. Wey, J. Goldhar, D.W. Rush, M.W. Chbat, G.M. Carter, and G.L. Burdge. Performance characterization of a harmonically mode-locked erbium fiber ring laser. *IEEE Photonics Technology Letters*, 7:152–154, 1995.

[49] E. Yoshida, Y. Kimura, and M. Nakazawa. Laser diode-pumped femtosecond erbium-doped fiber laser with a sub-ring for repetition rate control. *Appl. Phys. Lett.*, 60:932–934, 1992.

[50] J.L. Zyskind, E. Desurvire, J. W. Sulhoff, and D.J. DiGiovanni. Spectral gain hole-burning in an erbium-doped fiber amplifier. *Optical Amplifiers and their Applications*, pages 56–59, 1990.